EVALUATING THE METAMORPHIC HISTORY OF THE COAST MOUNTAINS BATHOLITH IN THE STIKINE RIVER AREA: ALASKA AND BRITISH COLUMBIA

by

SAVANNA GUTAPFEL

HAROLD STOWELL, COMMITTEE CHAIR
MARGARET RUSMORE
DELORES M. ROBINSON
SAMANTHA HANSEN

A THESIS

Submitted in partial fulfillment of the requirements for the Degree of Master of Science in the Department of Geological Sciences in the Graduate School of The University of Alabama.

TUSCALOOSA, ALABAMA

2023

ABSTRACT

The Coast Mountains batholith stretches more than 1,700 km along the western edge of North America and preserves a record of terrane amalgamation and magmatic arc processes. I present garnet Sm-Nd ages and pressure, temperature, time (P-T-t) paths for rocks along a transect crossing the Coast Mountains batholith near the Stikine River and Wrangell, AK. These sample locations straddle the Coast Shear Zone (CSZ): a fundamental, arc-parallel crustal break west of the batholith. The three new garnet Sm-Nd ages for metamorphism are 86.5 ± 3.6 (n=5) and 95.3 ± 4.8 (n=6) Ma in the Western Metamorphic Belt (WMB), and 57.0 ± 0.7 (n=6) Ma in the Eastern Metamorphic Belt (EMB). These ages, coupled with associated P-T-t paths provide new constraints on the plutonic and metamorphic history across the Coast Mountains. The WMB, marked by kyanite and staurolite zone mineral assemblages, was metamorphosed at 7.5 ± 1 kbar and 600-650°C between 86 and 95 Ma. Metamorphic conditions in the EMB are constrained by sillimanite replacing andalusite, and the P-T-t path indicates garnet growth at pressures from 4 to 6 kbar and temperatures from 550 to 650°C at ~57 Ma. These results indicate that garnet growth and cooling below garnet growth temperatures was ~30 million years earlier in the WMB than in the EMB. The metamorphic pressure estimates require > 10 km more exhumation in the WMB, which must have occurred significantly earlier in this area than further east. The new metamorphic data can be explained by exhumation due to focused uplift west of the CSZ and/or west-side-up tilting of the batholith ~80 Ma. This was followed by lesser amounts of exhumation in the central and eastern parts of the batholith.

DEDICATION

This thesis is dedicated to Lynne, Ellie and Ollie. None of whom contributed; all of whom inspired.

LIST OF ABBREVIATIONS AND SYMBOLS

Coast Mountains Geologic Abbreviations:

CMB	Coast Mountain Batholith
AK	Alaska
BC	British Columbia
CSZ	Coast Shear Zone
WMB	Western Metamorphic Belt
EMB	Eastern Metamorphic Belt

Mineral Abbreviations after Kretz (1983):

Grt	Garnet
Ky	Kyanite
Sil	Sillimanite
And	Andalusite
Bt	Biotite
Msc	Muscovite
Chl	Chlorite
Czo	Clinozoisite
Rt	Rutile
Ilm	Ilmenite
Pl	Plagioclase
Qtz	Quartz
Hbl	Hornblende

Garnet End Member Abbreviations:

Alm	Almandine (Fe)
Grs	Grossular (Ca)
Prp	Pyrope (Mg)
Sps	Spessartine (Mn)
Mg #	Magnesium number (Mg/Fe+Mg)

ACKNOWLEDGEMENTS

I would like to formally thank everyone who has been a source of knowledge, motivation and guidance throughout not only my completion of this thesis but those who guided me to this point in my academic career. Dr. Harold Stowell is mostly to thank (and blame), as he has been an unimaginable mentor throughout my graduate degree in all aspects of science, academia, research, life, and Colorado weather. I would also like to thank my committee members, Dr. Margaret Rusmore, Dr. Delores Robinson, and Dr. Samantha Hansen for their expertise, knowledge, guidance and time invested in editing this thesis. I would also like to thank my friends in the RadIs laboratory, Hannah Dickson, Ian Anderson and Dr. Elizabeth Bollen for mentoring and guiding me through this degree process. Robert Holler, of the Alabama Analytical Research Center, who not only trained me on the EPMA, but also helped sort out many technical issues during my use of that instrument; and Taylor Woods, who also contributed by correcting numerous, albeit user error, technical issues.

I'm also thankful for the financial support I received while completing this thesis which includes: The University of Alabama Research and Travel Fund, The W. Gary Hooks Endowed Geology Fund, the Geological Sciences Advisory Board for summer fund support, and The Graduate Council Fellowship for years of support through multiple teaching assistantships, which provided not only funding, but valuable teaching experiences.

CONTENTS

LIST OF TABLES

LIST OF FIGURES

INTRODUCTION

The Coast Mountains along the northwestern coast of North America are underlain by the long-lived Coast Mountains batholith (CMB), which extends more than 1700 km from the Yukon territory of Canada, through southeastern (SE) Alaska and British Columbia (BC), to north-central Washington State (Fig. 1). Plutons in the batholith provide an excellent laboratory for understanding magmatism, metamorphism, and tectonic processes in continental arcs because exhumation varies along strike, pluton ages vary along and across strike, and the mountains are deeply incised by glaciers and rivers, providing excellent exposures (e.g., Woodsworth et al. 2020).

The central core of plutons in the CMB is flanked by semi-continuous belts of metamorphic rocks to the east and west (Fig. 1). The metamorphic belt extending along the western flank, hereafter referred to as the Western Metamorphic Belt (WMB), is the most continuous and extensive belt with evidence for three major metamorphic events. The metamorphic belt extending along the eastern flank, hereafter referred to as the Eastern Metamorphic Belt (EMB), is less extensive, likely discontinuous along strike, and less well understood. This thesis is part of an effort to better understand the metamorphic and tectonic history of the CMB through integrated metamorphic, igneous, and structural studies along a transect across the batholith in the Stikine River area from near Wrangell, Alaska to near the location of sample 19EBBC06 (Fig. 2).

The goals of this thesis include identification of high-pressure rocks and large magnitude post-metamorphic faults and determination of metamorphic ages along the Stikine transect. Preliminary garnet Samarium (Sm) – Neodymium (Nd) geochronology and metamorphic pressure-temperature-time (P-T-t) paths for the EMB and WMB are presented. The new results include: 1) confirmation of regional metamorphic ages in the WMB, 2) new garnet Sm-Nd ages for metamorphism in the EMB, and 3) insights on the vertical displacements across the Coast Shear Zone (CSZ) and central batholith in the Stikine River area.

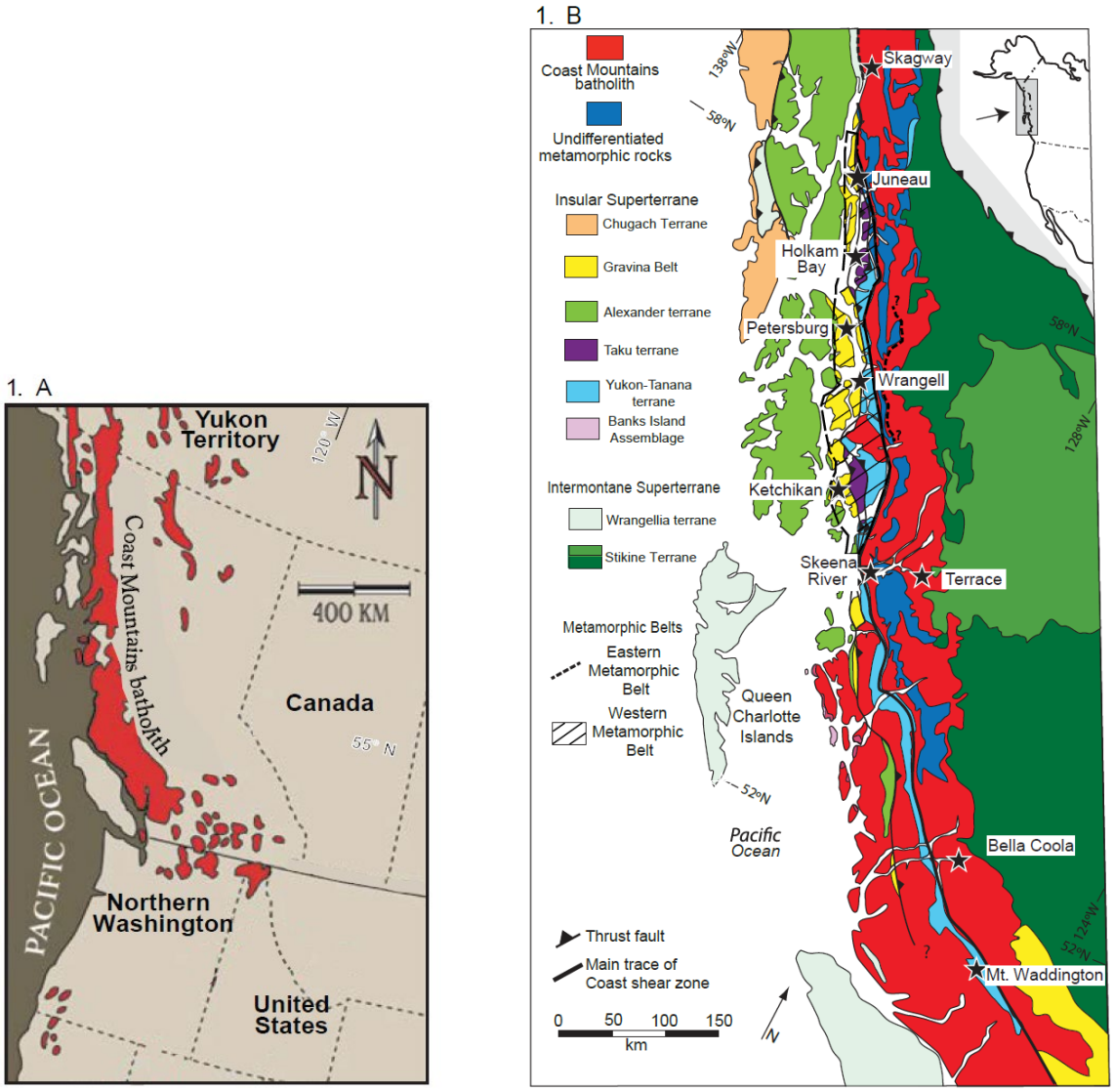

Figure 1. Generalized geologic map of the CMB region. (A) Generalized geologic map of the CMB and associated metamorphic rocks from Mt. Waddington to Skagway, indicating superterranes, terranes and the extents of the WMB and EMB near the Stikine River. Modified from Cecil et al. (2011) and references therein. (B) Continental extent of the CMB from the Yukon territory to Northern Washington State. Modified from Woodsworth et al. (2020) and references therein.

Geologic Background

The Coast Mountains are the eroded roots of a magmatic arc that was constructed by a collisional orogenic belt, formed from a series of island arcs that accreted to the North American plate (Monger et al., 1982). The batholith intrudes two composite tectonostratigraphic terranes: the Intermontane (east) and Insular (west) superterranes (Fig. 1). Metamorphic rocks, comprising deformed rocks of the superterranes, record this history of terrane accretion and magma emplacement. The CSZ, locally called the LeConte Bay Shear Zone in southeast Alaska, parallels the central batholith between the WMB and the central batholith (Fig. 1). The CSZ is a several kilometer wide zone of subvertical fabrics and faults with a polyphase history, which has been interpreted as transpressional with significant vertical displacements (e.g., Rusmore et al., 2001; Rubin et al., 1990; Chardon et al., 1999; Klepeis et al., 1999). Wide-angle seismic studies from the ACCRETE project confirm a ~5 km offset of the Moho at a depth of ~25 km below the CSZ (Morozov et al., 2001). Rubin et al. (1990) describe mid-Cretaceous west-vergent thrust faults distributed along strike throughout the Coast Mountains to represent the boundary between the Intermontane and Insular superterranes and obscured to the north by the Coast Plutonic Complex. Morozov et al. (2001) interpret the mid-Cretaceous thrust faults in the WMB to be truncated by possibly later strike-slip displacements on the CSZ, and they suggest that crust in the central batholith was thickened by voluminous magmatism. McClelland (1992) interprets the CSZ as the Tertiary boundary between the Alexander and Taku terranes. Rusmore (2001) describes the CSZ as a ductile reverse fault of continental scale that is 55-65 Ma, 2-11 km wide and includes synkinematic plutons.

The WMB includes parts of the Alexander and Wrangellia terranes and the overlying Gravina belt, which together comprise the Insular superterrane and parts of the Yukon-Tanana

terrane (Fig. 1). The Alexander terrane is composed of Neoproterozoic to Silurian metaigneous and metasedimentary rocks, representative of an island arc lacking continental influence (Gehrels & Saleeby, 1987; Cecil et al., 2011). The Wrangellia terrane includes upper Paleozoic and Mesozoic rocks and is characterized by low-grade metamorphic flood basalts, sedimentary rocks, and pillow basalts, which are attributed to Triassic rifting (Monger et al., 1992). The Gravina belt (Fig. 1) comprises a magmatic arc dominated by Jurassic to Cretaceous volcaniclastic rocks and overlying felsic and mafic metavolcanic rocks (Yokelson et al., 2015; Berg et al., 1972). Gravina belt rocks lie stratigraphically above the Alexander terrane to the west and the Yukon-Tanana terrane to the east; however, the contacts between these rocks are complicated by numerous plutons and a series of thrust faults. The Yukon-Tanana terrane is of Proterozoic to Paleozoic age and is composed of metasedimentary rocks and metavolcanics rocks that are intruded by tonalite, granodiorite, and granite of the central batholith. Largely resulting from the numerous plutons, the Yukon-Tanana terrane boundaries in the WMB and central batholith are poorly known (McClelland, 1992). The Yukon-Tanana and Stikine terranes to the east are members of the Intermontane superterrane (Fig. 1), which crops out east of the Coast Mountains. The Stikine terrane consists of Triassic to Jurassic magmatic arc assemblages, overlain by marine sedimentary strata. McClelland et al. (1992) and Cecil et al. (2011) suggest that the Stikine terrane rocks were deposited on the Yukon-Tanana terrane.

In the WMB, metamorphism resulted in sub-greenschist to upper amphibolite facies rocks from west to east toward the plutonic core of the batholith (e.g., Stowell, 1989; McClelland et al., 1990). The three major metamorphic events that affected and shaped the WMB are summarized in Table 1. The WMB is characterized by a steep metamorphic gradient, with the highest-grade rocks on the east, closest to the CSZ, inverted metamorphic isograds, and a wide

subvertical zone of strongly deformed rocks in the CSZ (Brew & Ford, 1978; Stowell & Hooper, 1990). The oldest recognizable metamorphism has been heavily overprinted by subsequent events, and few characteristics of the original metamorphism remain. This event was likely associated with a west-vergent, Mid-Cretaceous thrust system and crustal thickening, which resulted in pre-101 Ma metamorphic mineral assemblages. M2 metamorphism (Table 1) was regional and reached peak metamorphic pressures of 8-10 kbar (Crawford et al., 1987; Stowell & Crawford, 2000; McClelland, 1990; Rubin et al., 1990). This regional metamorphic event is synchronous with ~90 Ma diorite pluton emplacement (Stowell & Crawford, 2000; Gehrels, 1990) and resulted in contact metamorphism. Because of their close timing, these two events are labeled as M2C, for the contact metamorphic event and M2R, for the regional metamorphic event (Table 1). The metamorphic event is syn-tonalite emplacement and resulted in contact metamorphism at~60 Ma. This contact metamorphism reached sillimanite zone at 5 to 6 kbar. (Stowell & Goldberg, 1997; Stowell & Tinkham, 2003).

Table 1. Summary of the WB=MB metamorphic events, modified from Stowell & Tinkham (2003); Stowell & Crawford (2000)

Metamorphic Event	Time (Ma)	Geologic Time	Pressure (kbar)	Metamorphic facies
M1 - Regional Metamorphism - crustal thickening	Pre 101	Exact timing unknown	3-6	Greenschist
$M2^{C}$- Contact Metamorphism	90-101	Mid-Cretaceous	<3.8-8	Amphibolite
$M2^{R}$- Regional Metamorphism - crustal thickening	85-90	Mid/Late-Cretaceous	~9	Upper Amphibolite
M3 - Contact Metamorphism	50-72	Tertiary	<6	Upper Amphibolite

In the Stikine River area of the WMB, Late Cretaceous to Paleocene metamorphism overprinted mid-Cretaceous metamorphism west of and within the CSZ. McClelland et al. (1990) interpret syn-kinematic emplacement of tonalite sill plutons within the CSZ along the western edge of the CMB. However, undeformed tonalite crosscutting the CSZ, with concordant zircon U-Pb ages of 59.5 ± 1 Ma, indicates that deformation ceased ~50 Ma. Further south, Rusmore and Woodsworth (2001) indicate that the CSZ marks the western edge of Tertiary metamorphism. P-T estimates from west of and within the CSZ range from 7 ± 1 to 12 ± 1 kbar and from 465 ± 50°C to 890 ± 50°C. Extensive mid-Cretaceous crustal shortening and Late Cretaceous-Paleocene pluton emplacement within the shear zone likely contributed to significant thickening of the crust (McClelland et al., 1991). Subsequently, the collapse of the overthickened crust was likely responsible, in part, for the rapid uplift of the WMB (McClelland et al., 1991). West of the CSZ, garnet Sm-Nd ages from the pluton aureole at Garnet Ledge indicate initial garnet growth at 89.9 ± 3.6 Ma and final garnet growth at 89 ± 1 Ma (Fig. 2). Garnet compositions, mineral assemblage diagrams (MAD), and thermobarometry indicate that peak conditions for garnet growth were 680 ± 50°C and 6.2 ± 1 kbar (Stowell et al., 2001).

East of the CSZ, the central batholith is dominated by three major generations of primarily tonalitic to dioritic plutons and lesser amounts of high-grade metamorphic rock. Gehrels et al. (1990) describe the western boundary of the batholith to be 83-58 Ma tonalitic plutons, the central portion of the batholith to be dominated by 59-58 Ma tonalities to granodiorite plutons, and the east-central part of the batholith to be comprised of 51-48 Ma granite to granodiorite plutons. The westernmost plutons, which border the WMB, are subvertical and sill-like in geometry with gneissic subvertical fabrics (Brew & Ford, 1981). These Late Cretaceous and Paleocene tonalities were previously called the foliated tonalite sill,

great tonalite sill, or CPC sill plutons (Brew & Ford, 1978; Ingram & Hutton, 1994). They include the Quottoon pluton along the Skeena River (Hollister & Andronicos, 2000) and the synkinematic tonalite at LeConte Bay mentioned above. East of the CSZ, towards the central batholith, Eocene plutons were emplaced into the upper crust post deformation (e.g., Sisson, 1985).

Rocks of the central CMB are best known from studies along the Skeena River, which describe a high-grade metamorphic core, the Central Gneiss Complex (CGC), as summarized in Woodsworth et al. (2020, and references therein). The CGC includes several orthogneiss bodies and metasedimentary rocks with evidence for metamorphism at ~750°C and >10 kbar. This complex underwent significant Paleogene exhumation, much of which was accommodated by the east dipping, eastside detachment with east-side-down displacement (e.g., Woodsworth et al., 2020). High pressure metamorphic rocks and large magnitude east-side-down displacements have not yet been identified elsewhere along the batholith (e.g., Bollen et al., 2022).

The tectonic and metamorphic history of the EMB is not well characterized. However, the most detailed information on the EMB is from the Mt. Waddington thrust belt, approximately 725 km south of the Stikine River, at ~50°45’ latitude, near Mt. Waddington (Fig. 1). Rusmore and Woodsworth (1994) describe a series of east-directed thrusts that resulted in an inverted metamorphic sequence. In this thrust belt, metamorphic grade increases from NE to SW and the highest grade sillimanite zone mineral assemblages were metamorphosed at 650-700°C and up to 7 kbar (Rusmore & Woodsworth, 1994). Bollen et al. (2022) present garnet Sm-Nd ages of 64 and 72 Ma, indicating that at least some of this metamorphism post-dates the earliest WMB metamorphism recorded in southeastern Alaska.

North of Mt. Waddington, near Terrace, BC and the Skeena River, EMB rocks locally reached andalusite zone, with areas of contact metamorphism around post-kinematic plutons reaching higher grade (Greenwood et al., 1991). Based on observations along the Skeena River, Pearson et al. (2017) interpret that the Stikine terrane was underthrust beneath the central CMB before 80 Ma. The metamorphic rocks exposed in the Skeena River area may extend northward; however, few detailed studies have been completed. Based on the occurrence of andalusite and sillimanite (Porter, 1992), metamorphic rocks on the east side of the batholith near the Stikine River, at ~56.5° latitude, did not reach the pressures documented near Mt. Waddington and in the WMB of SE Alaska. Porter (1992) identifies two deformation events in rocks from Elbow Mountain in the EMB: the earliest is interpreted as syn-tectonic, and the second as late syn-tectonic or post-tectonic (Fig. 2). The first deformation event accompanied metamorphism and is associated with the formation of S1 cleavage that trends N-NW with east dipping cleavage and compositional banding. The second deformation event deforms S1 features into NW trending, overturned folds that dip to the NE. The second of the two metamorphic events peaked at lower amphibolite facies, produced garnet, andalusite and sillimanite mineral assemblages, and was interpreted by Porter (1992) to result from Early Jurassic pluton emplacement. Few ages have been published for these rocks; however, recently published U-Pb zircon analysis yield ages ranging from 53-59 Ma (Aleksey, 2020). This, along with preliminary Argon-Argon ($^{40}Ar/^{39}Ar$) and Potassium-Argon (K/Ar) ages from amphibole and biotite samples near Elbow Mountain that are between 58 and 51 Ma (Cecil, unpublished), indicate that metamorphism and subsequent cooling was younger than initially inferred by Porter et al. (1992).

Overall, published data on metamorphism in the CMB indicate distinct variations, both along and across strike. Peak metamorphism in the WMB and kyanite zone metamorphism in

the central batholith or CGC began before 90 Ma (e.g., McClelland et al., 1991; Stowell & Crawford, 2000; Rusmore et al., 2005; Wolf et al., 2010), earlier than peak metamorphism documented in the Mt. Waddington thrust belt. Although metamorphism in the central batholith is poorly known, high-pressure metamorphism has not been identified outside the Skeena River and adjacent areas. While Porter (1992) describes two closely related metamorphic events in the EMB near the Stikine River, precise ages for peak metamorphism are undocumented. Therefore, the additional data, including garnet Sm-Nd ages, peak metamorphic P-T estimates, and tentative P-T-t paths, presented in this thesis will further constrain the metamorphism and plutonism in the northern portion of the CMB. This, combined with data available from the southern sections of the CMB (e.g., Skeena fold and thrust belt, Mt. Waddington fold and thrust belt and the southern extent of the WMB), will allow construction of a more complete tectonic model for the Coast Mountains.

Research Objectives

The Stikine and Iskut River regions are ideal for studying metamorphism across the CMB and the CSZ because they have eroded through the Coast Mountains and provide a readily accessible transect to study medium to lower crustal metamorphism (Figs. 1-2). This study utilizes rocks from the Stikine transect, through the CMB from Wrangell to north of the Iskut River, to establish the first set of garnet growth ages across the entire CMB and is one of the first studies to compare the WMB and EMB directly adjacent and across the CSZ north of the Skeena River. This thesis has 4 objectives:

1. To calculate new garnet Sm-Nd ages representative of regional metamorphism across the CMB,
2. To construct P-T-t paths for these rocks using MAD and thermobarometry,
3. To compare the timing and P-T-t paths of metamorphism across the CMB in the Stikine River area to evaluate tectonic models for the CMB, and
4. To utilize the garnet ages and P-T-t paths for the WMB and EMB to evaluate displacements across the CSZ.

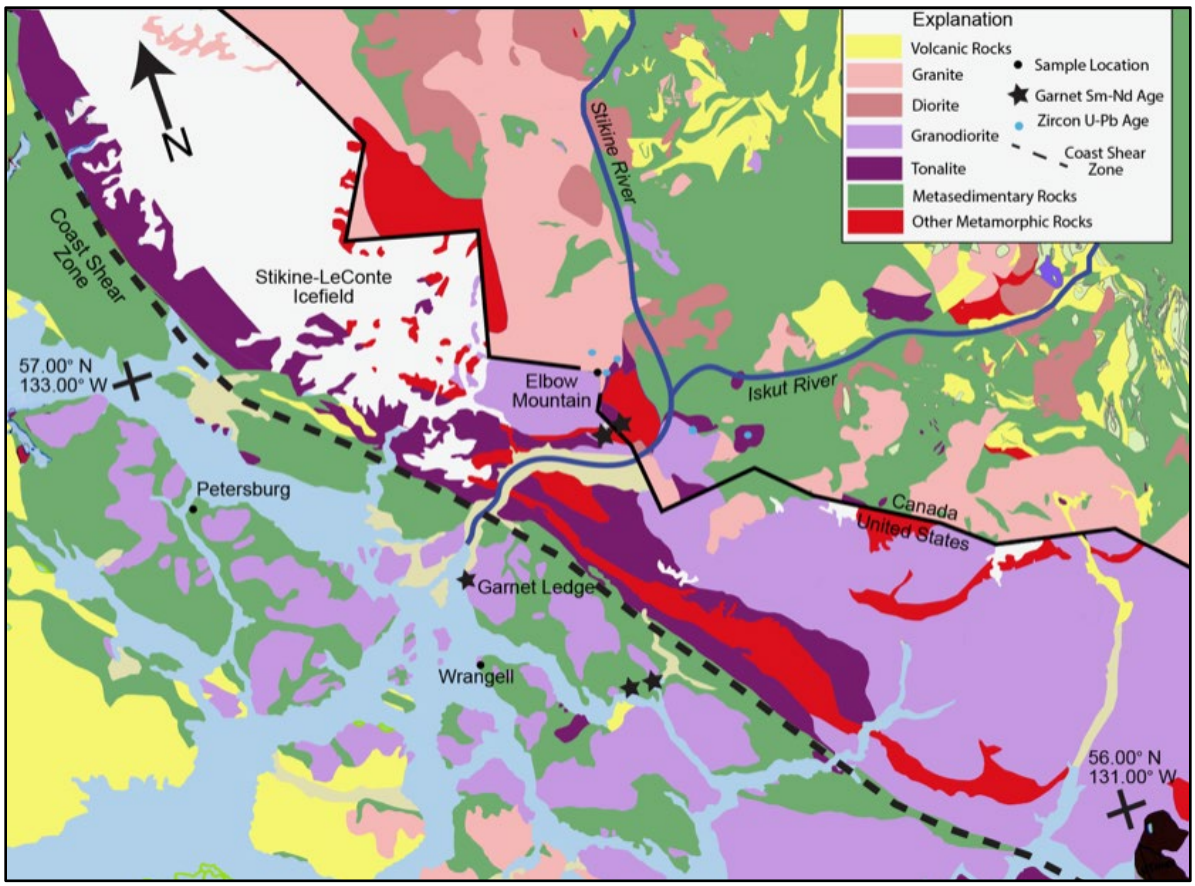

Figure 2. Simplified geologic map of the CMB, the WMB, and the EMB in the Stikine River area of southeast Alaska and adjacent BC. This map includes the general distribution of rocks, the CSZ, the Stikine River, and other major waterways (modified from Gehrels & Berg, 1992; Cui et al., 2017). The apparent granite-granodiorite contact at the international border both south and north of the Stikine River results from variations in map units and descriptions from different authors.

METHODS

Samples from the WMB were collected in 1995 by Harold Stowell and include garnet-biotite schist from Eastern Passage near Wrangell, AK. Samples east of the CSZ were collected in 2019 from BC by Elizabeth Bollen, Margaret Rusmore and Harold Stowell and include garnet-biotite schist representative of the metamorphic rocks east of the CSZ near Elbow Mountain and the Stikine River. The current research builds on mineralogical and textural observations in hand samples and thin sections. Thin sections were analyzed under both plane polarized light (PPL) and cross polarized light (XPL) to identify minerals based on their optical characteristics. This allowed selection of samples appropriate for garnet Sm-Nd geochronology and electron probe microanalysis.

Whole rock analysis

Whole rock compositions are used for geochemical characterization and as input for construction of MAD. Portions of each sample were selected from homogeneous areas of the samples (i.e., no internal compositional banding, etc.). Samples were selected and powdered using a carbon steel ring and puck mill in the SPEX Shatterbox at The University of Alabama. Powders were analyzed by X-ray fluorescence (XRF) at Activation Laboratories (Actlabs) and at Franklin and Marshall Laboratory (https://www.fandm.edu/stan-mertzman/xrd-and-xrf-laboratory). Comparison of whole rock values to average pelite compositions were used to identify anomalous compositions, which may stabilize less common minerals during metamorphism.

Garnet Sm-Nd geochronology

Garnet Sm-Nd dating was chosen because this allows age estimates to be combined with P and T estimates from the same mineral. Garnet works well for the isochron dating technique because it fractionates Sm over Nd more than other minerals and therefore allows for a precise age to be determined (e.g., Baxter & Scherer, 2013). Sm and Nd are both Rare Earth Elements (REE) and relatively small amounts are present in garnet; however, Sm is preferentially incorporated into garnet because it has a slightly smaller ionic radius. This element also has several long-lived radioactive isotopes, including ^{147}Sm, which decays to ^{143}Nd at a measured rate of 6.54×10^{-12} year^{-1}. Garnet geochronology is based on the following relationship:

$$\frac{^{143}Nd}{^{144}Nd} = \left(e^{\lambda t} - 1\right)\left(\frac{^{147}Sm}{^{147}Sm}\right) + \left(\frac{^{143}Nd}{^{144}Nd}\right),$$

where t is time, λ is the decay rate (6.54×10^{-12} /yr), and ^{143}Nd/^{144}Nd is the initial daughter isotope ratio. The above relationship is based on several assumptions. First, all minerals in the rock are assumed to have had the same, original ^{143}Nd/^{144}Nd ratio. Second, it is assumed that all radioactive ^{147}Sm decays to the stable ^{143}Nd isotope, which will decrease the ^{147}Sm/^{143}Nd ratio and will increase the ^{143}Nd/^{144}Nd ratio. Finally, it is assumed that the system is closed, such that there is no Sm or Nd exchanged with other minerals present in the rock. The above relationship can be used to solve for time:

$$t = \frac{1}{\lambda}\ln((^{143}Nd/^{144}Nd) - (^{143}Nd/^{144}Nd)i\,/(^{147}Sm/^{144}Nd) + 1)$$

This decay scheme, combined with isotope ratios for rock and mineral aliquots in equilibrium with variable Sm/Nd ratios, results in a linear relationship or isochron, where the x- and y-values are defined by ^{147}Sm/^{144}Nd and ^{143}Nd/^{144}Nd, respectively, and ^{144}Nd is used as the

reference isotope. Isotope dilution, or the process of spiking samples with a known value of a reference isotope, allows determination of the elemental concentrations in addition to the isotope ratios.

Garnet aliquots, whole rock, and matrix (i.e., whole rock samples with the garnet removed) samples are used to construct isochrons. The higher Sm/Nd in garnet results in higher radiogenic ^{143}Nd and a higher ^{143}Nd /^{144}Nd ratio in the aliquots compared to those for whole rock and matrix samples. Garnet aliquots were chosen based on various characteristics, including crystal size and the amount of included minerals. All samples had relatively small garnets, <2 mm, and were therefore analyzed as bulk garnet only.

Sample preparation

Samples for garnet Sm-Nd geochronology were selected from the most euhedral and inclusion-free garnet available that were representative of the sample. Garnet aliquots were crushed with an agate mortar and pestle and were sieved between 100 and 200 mesh. Garnet fragments were then handpicked for cleanliness in isopropyl alcohol under a reflected light microscope. This process removed mineral inclusions to ensure that the garnet aliquots were as mechanically clean as possible.

The mechanically clean garnet aliquots were then chemically cleaned by leaching them in several acids to remove any remaining mineral inclusions. Samples were first leached in 120°C $HN0_3$ for three hours, were cleaned with nanopure water, and then were leached in 120°C HF. HF leaching times varied, ranging from 35 to 80 minutes, based on the total mass of each aliquot, the estimated amount of mineral inclusions, and whether or not the aliquot was “picked” to remove inclusions mechanically before tackling them chemically. Finally, aliquots were leached in hot $HClO_4$ for 90 minutes before being evaporated and rinsed with nanopure water once more.

The garnet samples were then powdered with an agate mortar and pestle and were weighed within 0.00005 g precision. A mixed Sm and Nd spike (University of North Carolina Basalt 19a) was added to each sample, using 70 ql of spike per 100 mg of sample for garnet aliquots and 200ql of spike per 25 mg of rock and matrix samples. All rock and garnet aliquots were then dissolved in a series of hot acids over several days. Dissolution begins with a combination of hot HF and HNO_3 at ~120°C for three days. This solution was then evaporated, and a series of varying concentrations of hot HCl were added and evaporated to convert remaining fluorides to chlorides. After dissolution, each garnet, matrix, and whole rock aliquot was run through a Poly-Prep Bio-Rad column to concentrate the REE cations. Subsequently, individual aliquots of Sm and Nd were separated from the bulk REE using MLA in silica columns. The final elutions were treated with aqua regia and two drops of phosphoric acid to remove the MLA as the samples evaporated.

Thermal Ionization Mass Spectrometry

Sm and Nd isotope ratios were determined on the VG Sector 54 Thermal Ionization Mass Spectrometer (TIMS) in The University of Alabama's RadIs Lab (https://radis.as.ua.edu). Nd was loaded onto a single center Re filament and was measured as NdO. The Nd isotopic ratios were measured in dynamic mode and with seven Faraday collectors. Sm was loaded on a single center Ta filament and was measured as a metal in static mode with five Faraday collectors. Sm and Nd ratios and elemental concentrations were calculated using isotope dilution methods. These isotopic ratios were then used to calculate isochrons using ISOPLOT R (Vermeesch, 2018).

Electron Probe Microanalysis

Mineral analyses were obtained with the JEOL 8600 Electron Probe Microanalyzer (EPMA) at The University of Alabama's Analytical Research Center (AARC). Energy Dispersive Spectroscopy (EDS) was used to collect Kα X-ray maps for one sample, 95AKEP04; however, the detector was unavailable for analysis of the other samples. EDS maps were obtained with 15 kv accelerating voltage and a 200-300 nA beam current. Backscatter electron (BSE) maps were collected for all samples with operational parameters of 15 kv of accelerating voltage and ~200 nA beam current. Wavelength Dispersive Spectroscopy (WDS) was used to collect quantitative analyses of garnet, biotite, muscovite, and plagioclase grains for thermobarometry. Six or more garnet core and rim points and a linear array of analyses across individual garnet grains were measured to characterize compositional zoning. Operational parameters for WDS point analysis are 15 kv of accelerated voltage and 20 nA beam current. A ~1 μm beam was used for garnet samples, and a 10 μm beam was used for biotite and plagioclase samples. Analyses were filtered for use based on stoichiometry and normalized weight percent oxide totals.

Thermodynamic modeling

The THERIAK-DOMINO modeling software (de Capitani & Brown, 1987; de Capitani & Petrakakis, 2010) was used to construct P-T MADs in Mn, Na, Ca, K, Fe, Mg, Al, Ti, Si, O (MnNaCaKFMASHT) composition space. This forward thermodynamic modelling utilizes mineral end member activity models compiled by Tinkham (2021), which were based on the Holland and Powell (1989) thermodynamic database (v. 5.5). All of the MADs were constructed using whole rock XRF data, which were adjusted by removing phosphorus and the associated Ca as apatite before input. Water content was approximated based on the minimum water necessary to stabilize the observed mineral assemblages as estimated from a water mol proportion versus

temperature model. By determining where the rock is saturated with water in respect to temperature in P-T space, the best estimation for content was determined by where the water saturation line intersects the mol proportion of water. Garnet end member compositional isopleths, calculated with THERIAK-DOMINO, were used to determine P-T estimates of garnet core composition. GASP and GABI thermobarometry was utilized to determine rim P-T conditions. Biotite and plagioclase grains touching or adjacent to the garnet grains were analyzed for thermobarometry.

Thermobarometry

Observed mineral compositions and mineral exchange/net-transfer thermobarometry were used to construct P-T-t paths. Mineral assemblages containing garnet were targeted for garnet-biotite Fe-Mg exchange thermometry, or GABI (Ferry & Spear, 1978), and garnet-aluminum-silicate-plagioclase (GASP; Ghent et al. 1979) were used to estimate peak P-T conditions in four samples chosen for this thesis and further described in the results. Biotite, plagioclase, and garnet rim compositions for GASP and GABI were selected from touching or adjacent grains.

P-T paths

Peak metamorphic mineral assemblages determined by petrographic analysis were plotted on the MAD to estimate the peak metamorphic conditions. Garnet end member core compositions were added to the MAD to estimate the early part of the P-T path close to initial garnet growth. Isopleths of garnet volume, modeled with THERIAK-DOMINO, were used to confirm the P-T path from core to peak, to determine (if possible) where the majority of garnet growth occurred, and to determine if garnet was consumed at any point along the path. Finally, GASP barometry and GABI thermometry were used to predict garnet rim growth conditions.

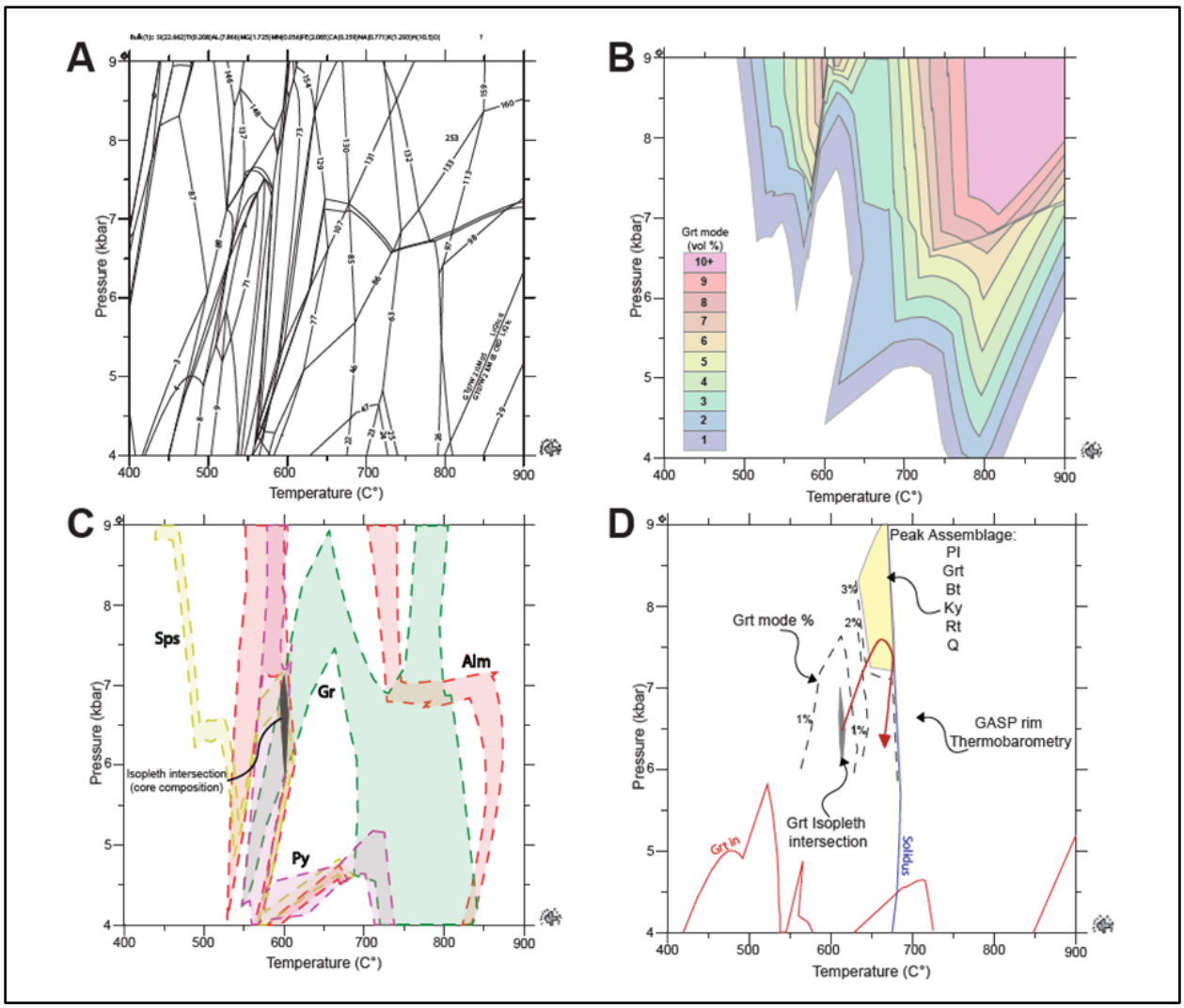

Figure 3. Components in P-T MAD construction. Example: 95AKEP04 A) Original output from THERIAK-DOMINO (DeCapitani & Petrikakas, 2010). All lines represent mineral, H_2O, or melt mode zero lines in P-T space. Each line is labeled and corresponds with a table of assemblages for each side of the mode zero line, also output from THERIAK-DOMINO. B) Garnet volume percent shown across P-T space. This shows the general trend in which garnet grew, as well as any locations garnet may have been consumed, to be compared with the final interpreted P-T path. C) Garnet core compositions, represented by end member isopleths. Each end member isopleth is indicated by a specific color. The grey box shows the intersection and therefore the interpreted P-T conditions for core growth. D) Final simplified P-T MAD with all P-T path components. The red arrow indicates the interpreted P-T path and shows garnet growth from core composition along increased garnet mode to peak assemblage. The prograde curvature in the path is constructed from the peak and post peak mineral assemblage stable fields, garnet modes, and in some samples, thermobarometry for mineral rim compositions.

RESULTS

The following section describes petrography, whole rock composition, mineral compositions, garnet Sm-Nd geochronology, and P-T-t path results of samples collected from the CMB, along the Stikine River transect in southeast AK and adjacent B.C

Table 2. Sample description and locations along the Stikine transect southeastern AK and adjacent B.C.

Sample Name	Location		Lat.	Long.	Description
95AKEP04	WMB	Eastern Passage	56.3633	-132.0070	Grt, Bt, Ky schist
95AKEP06	WMB	Eastern Passage	56.3579	-132.0183	Grt, Bt, St schist
19EBBC03A	EMB	Elbow Mountain	56.7021	-131.8644	Grt, Bt schist
19EBBC03B	EMB	Elbow Mountain	56.7021	-131.8644	Grt, Bt schist
19EBBC06A	EMB	Elbow Mountain	56.7046	-131.8589	Grt, Bt, Sil schist
19EBBC06F	EMB	Elbow Mountain	56.7046	-131.8589	Float sample- Grt, Bt, And, Sil schist

.

WMB: Sample 95AKEP04

The following section describes the results from Sample 95AKEP04, the easternmost sample in the WMB.

Petrography

Sample 95AKEP04 is a garnet-kyanite-biotite schist collected from an inlet adjacent to the Eastern Passage, just east of Wrangell Island (Fig. 2). This sample contains garnet, kyanite, biotite, muscovite, staurolite, plagioclase, quartz, rutile, and opaques. Textural relationships, including anhedral staurolite, muscovite overgrowing foliation, and kyanite, indicate that the peak metamorphic assemblage is garnet, kyanite, biotite, rutile, quartz, and plagioclase. Garnet grains are euhedral, 0.7-1.2 mm in diameter, and contain very few inclusions of quartz. Kyanite grains are large, bladed crystals, ranging from 3-6 mm. Two stages of kyanite growth are interpreted: one set of grains that are 4-6 mm maximum in dimension and that are anhedral, and a second set of grains that are subhedral, slightly smaller in size (3-5 mm) and that overgrow the anhedral kyanite grains. Small, anhedral staurolite grains are out of equilibrium and are interpreted as being resorbed. Biotite is aligned along the foliation (Fig. 4).

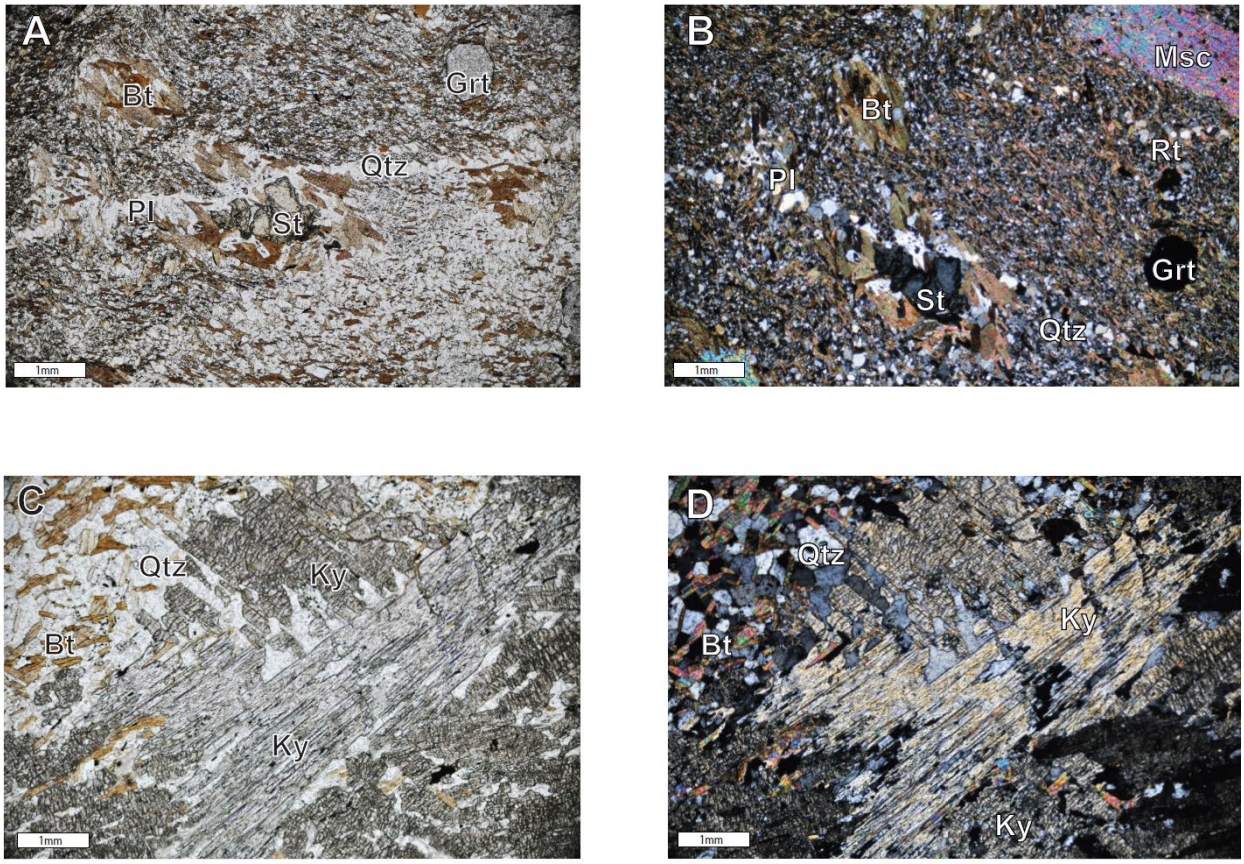

Figure 4. Photomicrographs of Sample 95AKEP04, from the WMB in Alaska. All photomicrographs are taken at 4x magnification. A) Plane polarized light image and B) cross polarized light image showing garnet, kyanite blades and matrix minerals. On panels C and D, two generations of kyanite blades are shown: the older generation (gen 1) are more subhedral with quartz and plagioclase inclusions, and the younger generation (gen 2) cross-cut the older grains and are much better preserved. C) Plane polarized light image and D) cross polarized light image of a euhedral garnet grain and a staurolite relic adjacent to kyanite grains.

Whole rock compositions

Sample 95AKEP04 is a pelite, with a composition similar to an average shale (Ague, 1991; Shaw, 1956). Compared to the Ague (1991) average pelite composition, Sample 95AKEP04 has a higher SiO_2 and P_2O_5, approximately equal Al_2O_3, and lower TiO_2, Fe_2O_3, MnO, CaO, Na_2O, and K_2O (Table 3). Kyanite and relict staurolite indicate that this sample is a high aluminum pelite (Spear, 1993). Table 3 summarizes the corresponding oxide concentrations.

Table 3. Rock compositions from the CMB along the Stikine transect, AK and B.C.

	Western Metamorphic Belt		Eastern Metamorphic Belt				Average Pelite - Ague 1991	
	95AKEP04	95AKEP06	19EBBC06A	19EBBC06F	19EBBC06A	19EBBC03B	Greenschist facies	Amphibolite facies
SiO_2	63.26	60.04	48.96	69.18	48.96	57.85	58.33	56.25
TiO_2	0.77	0.86	2.92	0.73	2.92	0.89	0.9	1.05
Al_2O_3	18.63	17.37	17.7	15.01	17.7	17.89	18.63	20.18
Fe_2O_3	7.66	9.4	14.5	5.64	14.5	9.52	8.06	9.31
MnO	0.12	0.108	0.304	0.037	0.304	0.303	0.29	0.18
MgO	3.23	3.94	5.18	2.24	5.18	2.89	3.01	3.23
CaO	0.99	1.39	5.67	1.34	5.67	6.24	1.5	1.54
Na_2O	1.11	1.96	3.56	1.69	3.56	0.63	1.59	1.8
K_2O	2.83	2.88	0.92	2.21	0.92	2.15	3.98	4.02
P_2O_5	0.24	0.27	0.8	0.11	0.8	0.48	0.18	0.19
Total	98.84	98.218	100.70	98.187	100.514	98.843	96.47	97.75

Mineral compositions

Garnet, plagioclase, and biotite grains were analyzed from Sample 95AKEP04. A ~1.2 mm garnet grain was analyzed first by a chemical map to determine relative elemental concentrations (Fig. 5). Those maps helped to determine the chemical center of the grain, allowing for further evaluation of compositional zoning using EPMA point analyses along a line crossing the grain. Additional point analyses were obtained from biotite and plagioclase adjacent to the garnet rim for GASP and GABI thermobarometry. Almandine and spessartine are strongly zoned, and pyrope and grossular are weakly zoned (Fig. 6). The garnet composition varies as follows: $almandine_{core} = 0.66$ to $almandine_{rim} = 0.72$; $spessartine_{core} = 0.17$ to $spessartine_{rim} = 0.07$; $pyrope_{core} = 0.13$ to $pyrope_{rim} = 0.15$; and $grossular_{core} = 0.04$ to $grossular_{rim} = 0.05$. Almandine, pyrope, and grossular gradually increase from core to rim, with magnesium numbers (Mg/(Mg+Fe)) following the pyrope zoning trend. Spessartine is zoned in a bell-shaped curve decreasing from the core outwards to the rim. Small decreases are observed in both the magnesium number and pyrope at the outermost rim of the garnet grain, ~ 0.2 mm from the rim. Tables 4-6 summarize the representative mineral analyses used for thermobarometry and garnet compositional zoning.

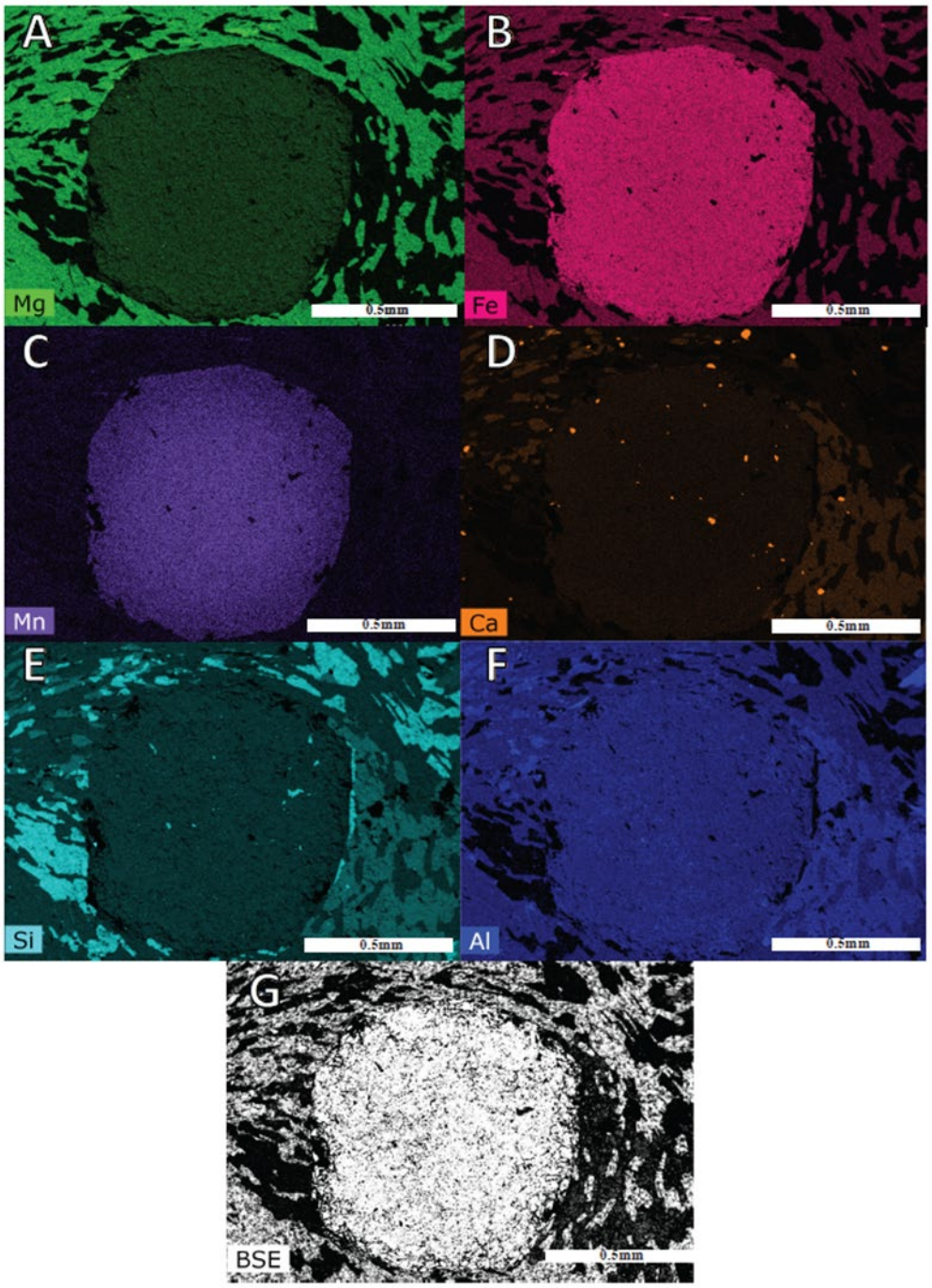

Figure 5. Kα X-ray intensity and BSE maps of a garnet grain in Sample 95AKEP04, showing major element zoning. A) Mg Kα X-ray map. B) Fe Kα X-ray map. C) Mn Kα X-ray map. D) Ca Kα X-ray map. E) Si Kα X-ray map. F) Al Kα X-ray map. G) BSE map.

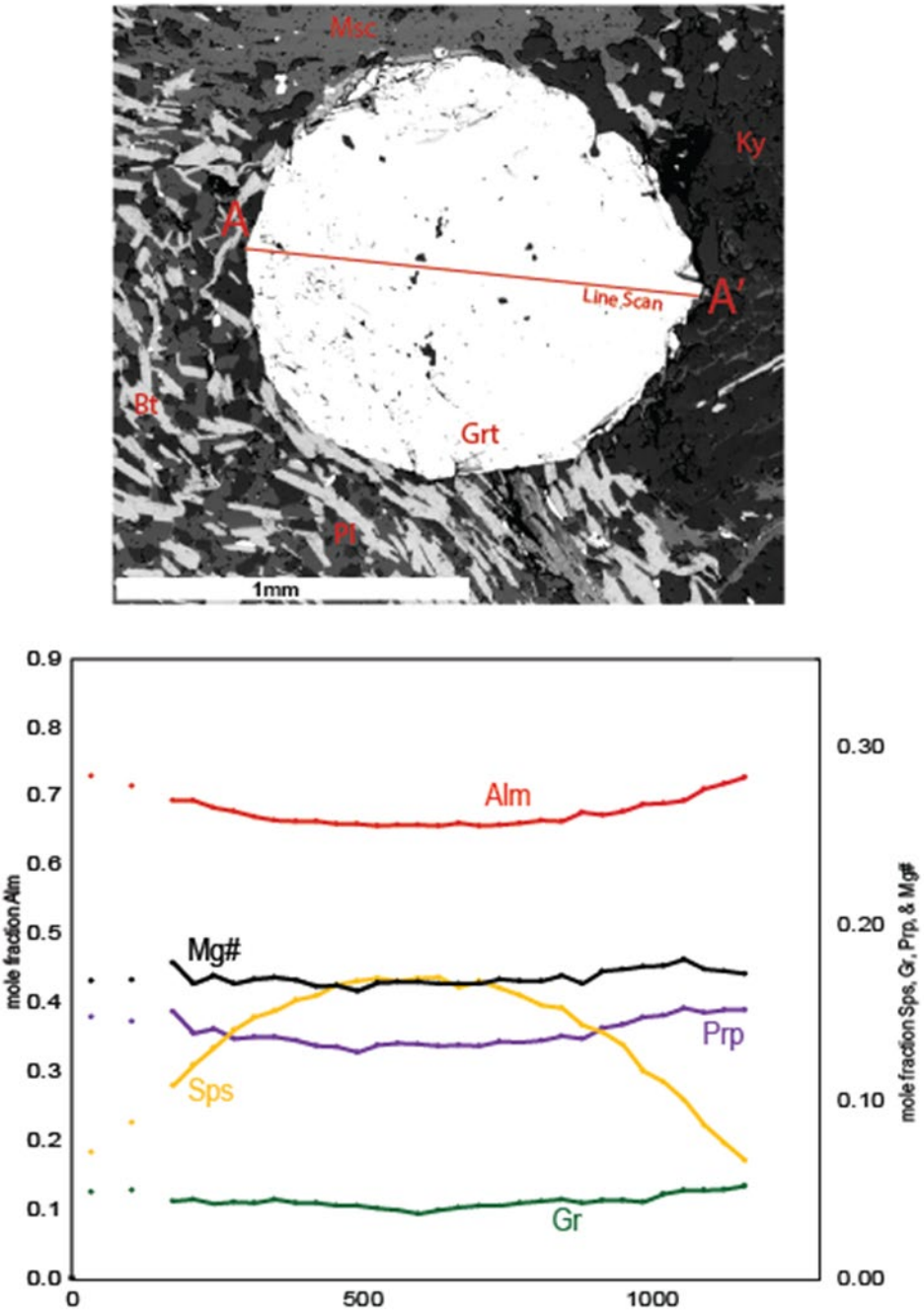

Figure 6. Garnet compositions in Sample 95AKEP04. A) BSE image of garnet, with line scan position indicated by profile A-A'. B) Garnet compositional zoning profile, plotting end member and magnesium number versus distance across the grain along profile A-A'. The line scan is based on 32 quantitative WDS point analysis.

Table 4. Representative garnet rim analyses from the Stikine transect.

	95AKEP04	95AKEP06	19EBBC03B
Wt %			
SiO_2	36.93	37.24	36.67
TiO_2	0.01	0.00	0.04
Al_2O_3	21.54	21.99	21.47
FeO	32.86	34.79	32.16
MnO	3.18	1.63	3.56
MgO	3.77	3.90	2.57
CaO	1.83	1.47	3.02
Total	100.12	101.01	99.49
Cations			
Si	2.962	2.955	2.967
Ti	0.000	0.000	0.002
Al	2.015	2.057	2.047
Fe	2.227	2.309	2.176
Mn	0.216	0.109	0.244
Mg	0.451	0.461	0.310
Ca	0.157	0.125	0.262
Total	8.030	8.016	8.008
End Members			
Mg #	0.168	0.167	0.125
Almandine	0.730	0.768	0.727
Pyrope	0.148	0.154	0.104
Spessartine	0.071	0.036	0.082
Grossular	0.051	0.042	0.088

Table 5. Representative biotite analyses from the Stikine transect.

	95AKEP04	95AKEP06	19EBBC03B
Wt %			
SiO_2	35.28	37.27	34.82
Al_2O_3	19.62	21.09	18.71
FeO	18.07	17.09	20.43
MnO	0.06	0.03	0.10
TiO_2	1.82	1.99	2.27
CaO	0.00	0.00	0.04
MgO	10.62	11.20	9.49
Na_2O	0.14	0.15	0.07
K_2O	8.41	8.31	8.10
H2O*	3.94	4.12	3.89
Total	97.96	101.25	97.93
Cations			
Si	2.686	2.710	2.683
Al	1.761	1.808	1.699
Fe	1.150	1.039	1.317
Mn	0.004	0.002	0.006
Ti	0.104	0.109	0.132
Ca	0.000	0.000	0.004
Mg	1.206	1.214	1.091
Na	0.020	0.021	0.010
K	0.817	0.771	0.796
H*	2.000	2.000	2.000
Total	7.748	7.673	7.738
End Members			
Mg#	0.512	0.538	0.453
Al IV	1.314	1.294	1.317
Al VI	0.447	0.518	0.383

* = calculated value

Table 6. Representative plagioclase analyses from the Stikine transect.

	95AKEP04	95AKEP06	19EBBC03B
Wt %			
SiO_2	60.09	62.49	n.d.
Al_2O_3	24.81	23.23	n.d.
FeO	0.18	0.20	n.d.
CaO	5.51	5.10	n.d.
Na_2O	7.00	9.80	n.d.
K_2O	0.06	0.07	n.d.
Total	97.66	100.88	n.d.
Cations			
Si	2.719	2.759	n.d.
Al	1.323	1.209	n.d.
Fe	0.000	0.008	n.d.
Ca	0.267	0.241	n.d.
Na	0.614	0.839	n.d.
K	0.004	0.004	n.d.
Total	4.928	5.058	n.d.
End Members			
Alb	0.694	0.774	n.d.
An	0.302	0.223	n.d.
Kspar	0.004	0.003	n.d.

Garnet Sm-Nd Geochronology

A garnet Sm-Nd isochron was constructed for Sample 95AKEP04 using four bulk garnet aliquots combined with matrix and whole rock aliquots. The garnet Sm-Nd age is 95.3 ± 4.8 Ma (2σ uncertainty), with a mean square weight derivative, or MSWD = 2.0 (Fig. 7). Sm and Nd isotope ratios and concentrations are summarized in Table 7 below. This MSWD value indicates possible complexity in the results. Further, the simple major element zoning in garnet and the lack of objective criteria do not permit definitive interpretation of the variability. It is speculated that the Gx >1 aliquot included mineral grains that were not removed during leaching.

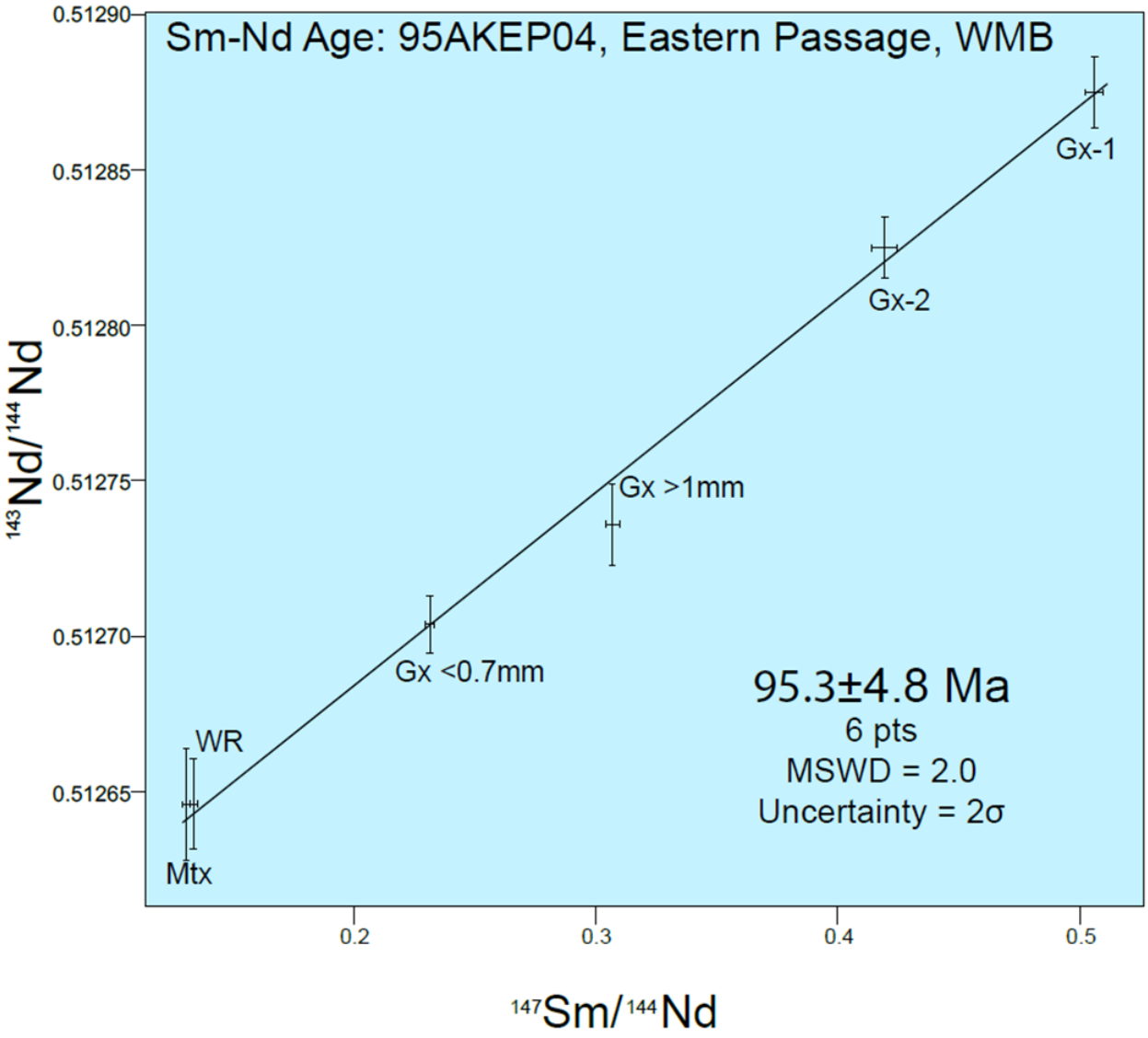

Figure 7. Sm-Nd isochron for garnet-biotite schist Sample 95AKEP04. Isotope ratios for four garnet aliquots, matrix, and whole rock samples yield an age of 95.3 ± 4.8 Ma with an MSWD of 2.0. Age result and all isotopic ratios are presented with 2σ uncertainties. Table 7 summarizes the corresponding isotope ratios.

Table 7. Garnet Sm/Nd isotopic data for rocks along the Stikine transect.

Table 7. Garnet Sm/Nd isotopic data for rocks along the Stikine Transect.

Sample	Weight (g)	$[Sm]_{ppm}$	$[Nd]_{ppm}$	$^{147}Sm/^{144}Nd$	2 SE	$^{143}Nd/^{144}Nd$	2 SE	Age±2σ	MSWD
95AKEP04								**95.3±2.8 Ma**	**2.0**
Gx <.7 mm	0.01917	1.350	3.520	0.2319	0.0017	0.512704	0.000008		
Gx >1 mm	0.02021	1.299	2.553	0.3077	0.0022	0.512737	0.000011		
Gx1	0.04140	1.342	1.603	0.5060	0.0035	0.512875	0.000010		
Gx2	0.03473	1.431	2.060	0.4201	0.0029	0.512825	0.000008		
Mtx	0.03013	3.266	15.119	0.1306	0.0009	0.512646	0.000015		
WR	0.02574	2.447	11.045	0.1340	0.0009	0.512646	0.000012		
95AKEP06								**86.5±3.6 Ma**	**2.2**
Gx <1mm	0.04350	1.296	2.180	0.3594	0.0025	0.512822	0.000011		
Gx 1mm	0.04328	1.346	1.683	0.4834	0.0034	0.512904	0.000010		
Gx >1mm	0.04861	1.333	1.262	0.6384	0.0045	0.512972	0.000014		
Mtx	0.02875	3.448	15.125	0.1378	0.0010	0.512702	0.000008		
WR	0.02606	4.748	21.321	0.1346	0.0010	0.512695	0.000008		
19EBBC03A								**56.7±0.7 Ma**	**0.9**
Gx1	0.02165	2.954	0.772	2.3148	0.0163	0.513427	0.000016		
Gx2	0.02008	2.796	0.690	2.4492	0.0174	0.513460	0.000033		
Gx3	0.03191	2.900	0.884	1.9829	0.0140	0.513309	0.000014		
Gx-UP	0.04143	2.750	0.539	3.0874	0.0219	0.513730	0.000018		
Mtx	0.02931	4.744	21.696	0.1322	0.0009	0.512624	0.000008		
WR	0.02794	4.137	18.293	0.1367	0.0010	0.512627	0.000008		
19EBBC06A								**NO AGE INTERPRETED**	
Gx-P	0.01918	6.554	12.742	0.3110	0.0020	0.512901	0.000008		
Gx-UP	0.06764	5.368	8.623	0.3764	0.0026	0.512931	0.000007		
Gc-P	0.03065	6.346	12.242	0.3134	0.0020	0.512877	0.000007		
Gx-UP-2	0.05989	6.031	10.204	0.3573	0.0024	0.512895	0.000009		
Gx1	0.03656	6.018	10.904	0.3337	0.0023	0.512886	0.000008		
Gx2	0.03074	5.950	10.344	0.3477	0.0023	0.512918	0.000009		
WR	0.02370	13.271	63.223	0.1269	0.0009	0.512822	0.000008		

P-T-t paths

The P-T MAD for Sample 95AKEP04 is presented in Figure 8. The combination of the garnet core P-T estimate, the peak mineral assemblage field on the MAD, and the rim P-T estimate from thermobarometry are used to construct a prograde P-T path that begins at ~600°C and 6-7 kbar, peaks at 640-670°C and 7-9 kbar, and based on garnet rim thermobarometry, continues to 600-700°C and 4.2-6.5 kbar. This path is supported by the predicted garnet percent volume increase from 0 to 4% from garnet core to peak conditions. Most of the garnet growth is predicted between core growth and peak assemblage with temperature and pressure increasing from 600 to 650°C and 6 to 7.5 kbar, respectively. The final stage of the path from peak to final P-T conditions predicted from thermobarometry is parallel to the garnet mode isolines. This is interpreted to result from rim equilibration with insignificant garnet growth.

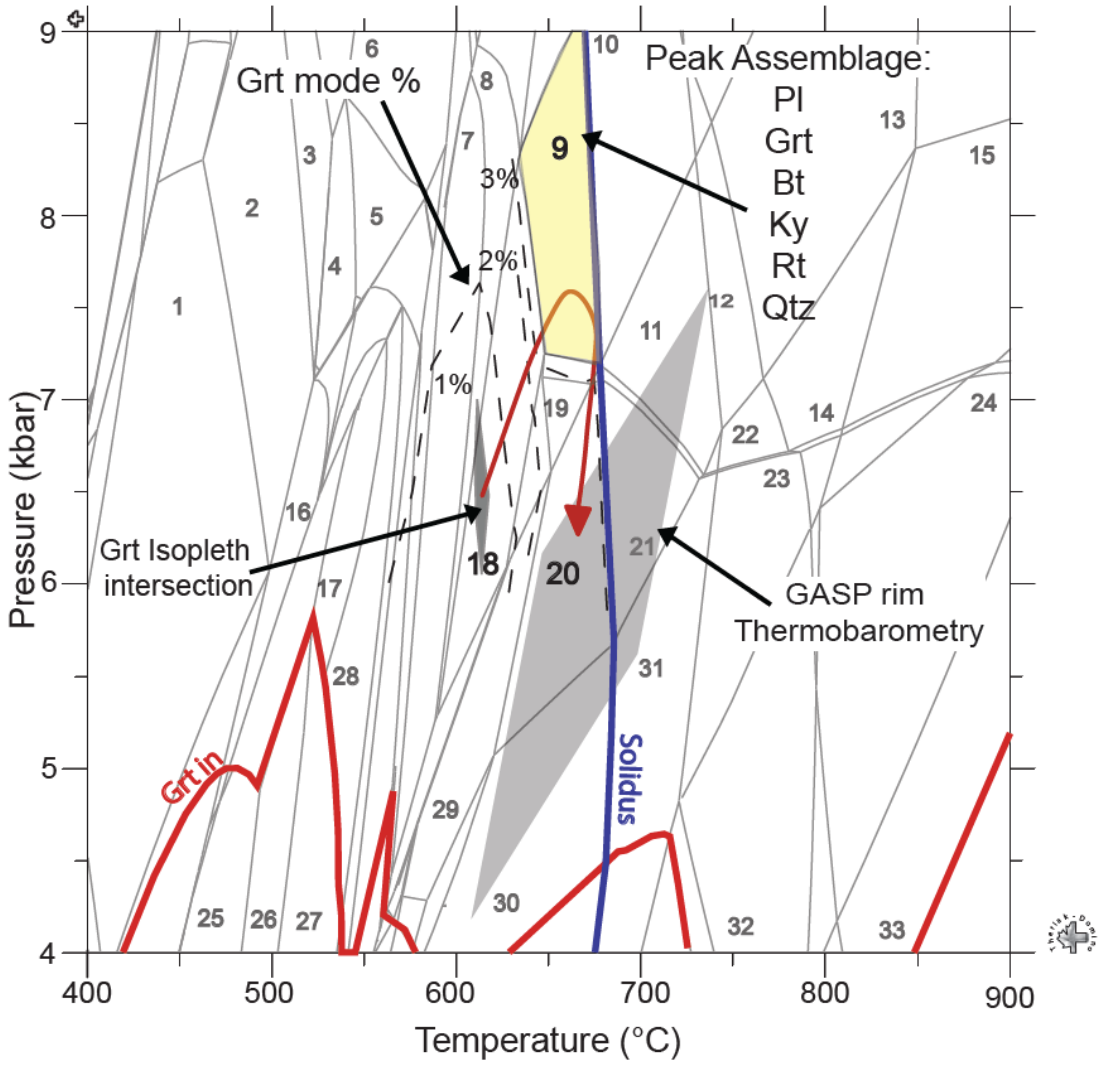

Major Mineral Stability Fields:

8. Grt, Bt, Ky, (2) WM, St, Rt, Pl, Qtz **9.** Grt, Bt, Ky, Rt, Pl, Qtz
10. Grt, Bt, Ky, Rt, Pl, Qtz, Liq **18.** Grt, Bt, Ky, Rt, St, Pl, Qtz
20. Grt, Bt, Pl, Ilm, Sill, Qtz

Figure 8. Simplified P-T mineral assemblage diagram for garnet-biotite schist Sample 95AKEP04. The yellow polygon shows the predicted stability of the observed peak metamorphic mineral assemblage: garnet, biotite, kyanite, plagioclase, quartz, and rutile. The dark gray polygon indicates the area of intersection for predicted garnet end member isopleths for the observed garnet core composition. Dashed black lines indicate the predicted garnet volume percentage. The light grey polygon indicates the P-T estimated garnet rim compositions based on GASP and GABI thermobarometry. The red arrow indicates the interpreted P-T path. All assemblages are plus water. Appendix 1 provides a complete listing of predicted minerals.

WMB: Sample 95AKEP06

The following section describes the results from Sample 95AKEP06, the westernmost sample in the WMB.

Petrography

Sample 95AKEP06 was collected from the westernmost location in the study area, ~2 km west of the Sample 94AKEP04 location site (Fig. 2), and it is a garnet-staurolite-biotite schist, containing garnet, staurolite, biotite, muscovite, rutile, and opaques. Garnet grains are ≤ 1.5 mm in size, are euhedral, and contain sparse inclusions of quartz. Biotite, plagioclase, and quartz form the dominant foliation. Large staurolite porphyroblasts, ranging from 3-5 mm, contain numerous quartz and plagioclase inclusions. Large muscovite grains crosscut the foliation and are interpreted to postdate deformation.

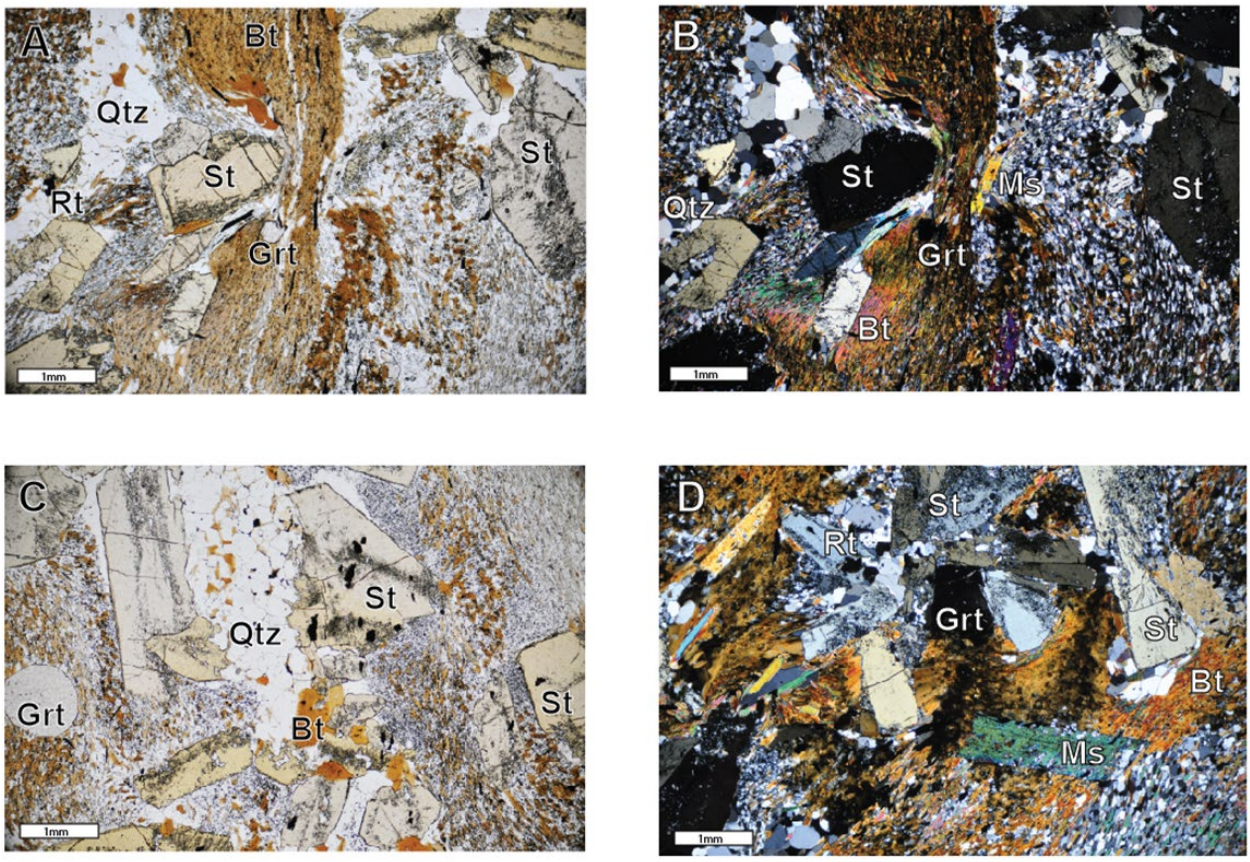

Figure 9. Photomicrographs of garnet-biotite-staurolite schist, Sample 95AKEP06, from the WMB in southeastern Alaska. A) Plane polarized light image and B) cross polarized light image showing garnet, staurolite, biotite porphyroblasts, and matrix minerals. The large staurolite grains are subhedral, with numerous inclusions of plagioclase and quartz. C) Plane polarized light image of a euhedral garnet grain and euhedral-subhedral staurolite grains, some of which are replaced by quartz. D) Cross polarized light image of subhedral garnet and staurolite and muscovite grains crossing the foliation, the latter of which are interpreted to postdate deformation.

Whole Rock Composition

Sample 95AKEP06 is a pelite with a composition similar to average amphibolite facies pelites (Auge, 1991). However, this sample is higher in SiO_2, MgO, Na_2O, and P_2O_5 and is lower in Al_2O_3, TiO_2, CaO, and K_2O compared to the average pelite. Total iron (as Fe_2O_3) and MnO concentrations are approximately equal to an average pelite. The high mode of staurolite is typically associated with high aluminum pelites (Spear, 1993); however, the lower than average Al_2O_3 indicates that staurolite was likely stabilized by other means, perhaps by trace concentrations of elements that were not analyzed for this study (e.g., zinc). Table 3 summarizes the associated oxide concentrations.

Mineral Compositions

Garnet and biotite grains were analyzed from Sample 95AKEP06. Garnet rim and adjacent biotite grains were analyzed for GABI thermometry. The 0.54 mm diameter garnet grain analyzed from this sample has compositional zoning from the core to the rim with the following compositions: $almandine_{core} = 0.74$ to $almandine_{rim} = 0.77$; $spessartine_{core} = 0.048$ to $spessartine_{rim} = 0.035$; $pyrope_{core} = 0.17$ to $pyrope_{rim} = 0.14$; and $grossular_{core} = 0.043$ to $grossular_{rim} = 0.041$. Relative to Sample 95AKEP04, this garnet is weakly zoned. Almandine increases from core to rim, and pyrope, spessartine, and the magnesium number decrease slightly from core to rim. Small increases in the spessartine zoning can be seen within ~0.05 mm from the rim. Tables 4-6 summarize the relevant mineral analyses.

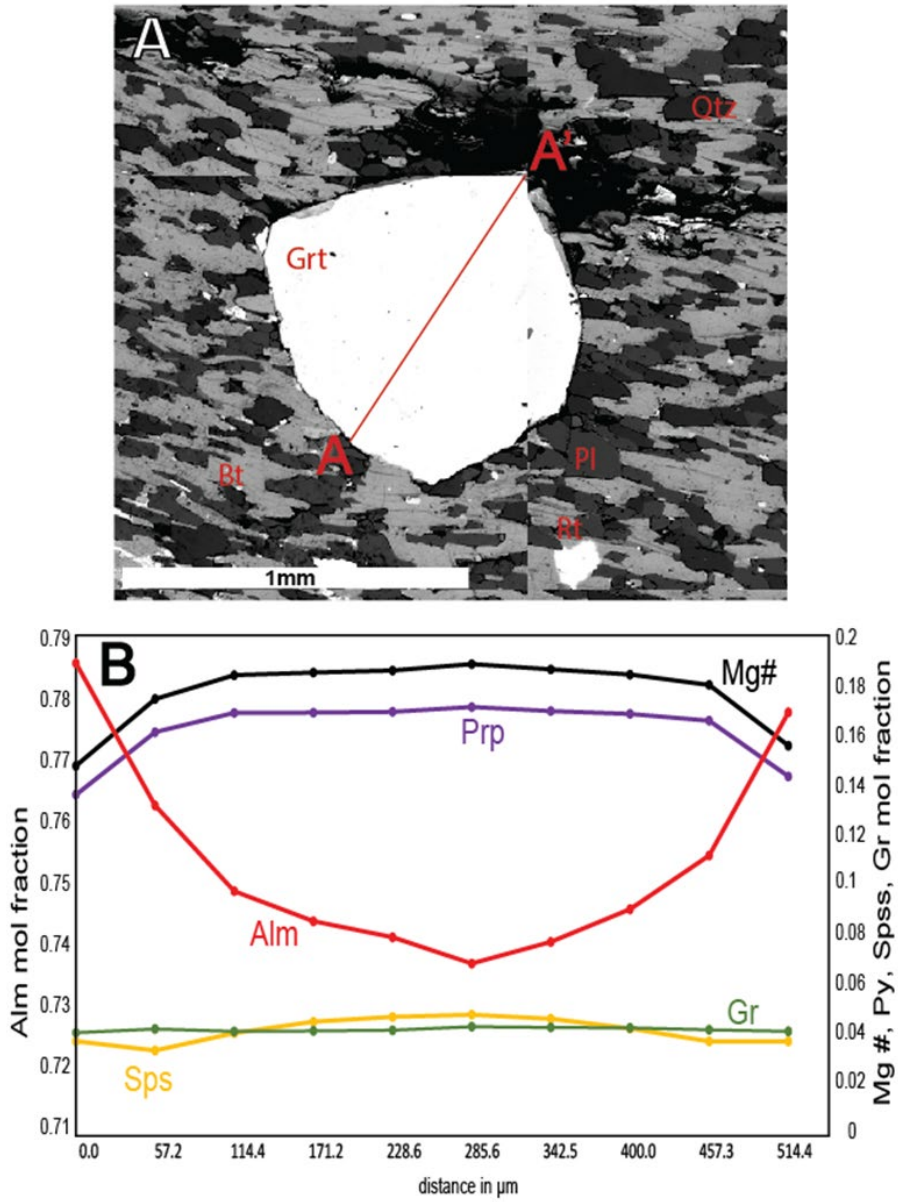

Figure 10. Garnet BSE map and compositional zoning profile for Sample 95AKEP06. A) BSE image of garnet, with profile A-A' indicating the line scan position. B) Garnet compositional zoning profile, showing end member mole fractions and magnesium number versus distance across the garnet along profile A-A'. The line scan includes 12 quantitative WDS point analysis. Tables 4-6 summarize the full mineral analyses.

Garnet Sm-Nd Geochronology

Garnet Sm-Nd isochrons are constructed using three bulk garnet aliquots combined with matrix and whole rock aliquots. The garnet Sm-Nd age for Sample 95AKEP06 is 86.5 ± 3.6 Ma (2σ uncertainty) with an MSWD = 2.2 (Fig. 11). Sm and Nd isotope ratios and concentrations are summarized in Table 7. The MSWD is high, and similar to the isochron for Sample 95AKEP04, the garnet aliquots cannot be logically interpreted as reflecting multiple ages or post growth re-equilibration.

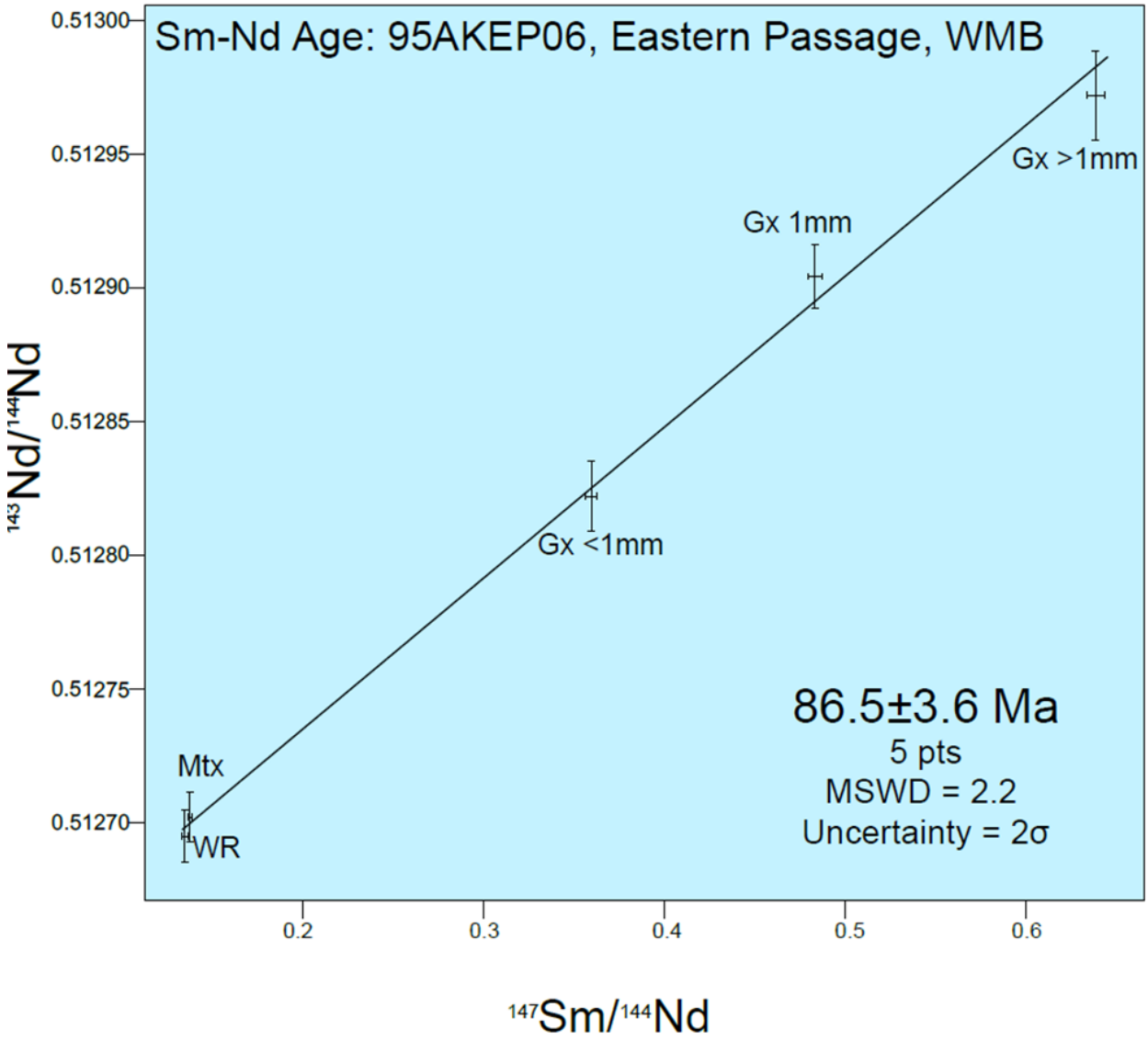

Figure 11. Sm-Nd isochron for Sample 95AKEP06. Isotope ratios for three garnet aliquots, matrix, and whole rock samples yield an age of 86.5 ± 3.6 Ma with an MSWD of 2.2. Age result and all isotope ratios are presented with 2σ uncertainties. Table 7 summarizes associated isotope ratios.

P-T-t path

The P-T MAD for Sample 95AKEP06 is presented in Figure 12. The combination of the garnet core P-T estimate, the peak mineral assemblage field predicted on the MAD, and the rim temperature estimate from thermometry are used to construct general P-T parameters indicative of a prograde path. Garnet core growth begins at 575-625°C and 6.75-7.75 kbar, and it peaks at 600-700°C and 7-8.5 kbar. The GABI thermometry exchange reaction predicts rim growth at 585 ± 50°C and is indicated by the light pink rectangle in Figure 12. This is interpreted as the final temperature P-T conditions because the garnet rim compositions are thought to result from post peak equilibration, indicated by downturns in iron and magnesium number along the rim. This P-T-t path is supported by predicted garnet percent volume increases from 2-6% along the path. Most of this garnet growth is predicted between the core and peak assemblage temperatures and pressures as they increased to 600-650°C and 6.75-8.5 kbar, respectively, at ~85.6 Ma.

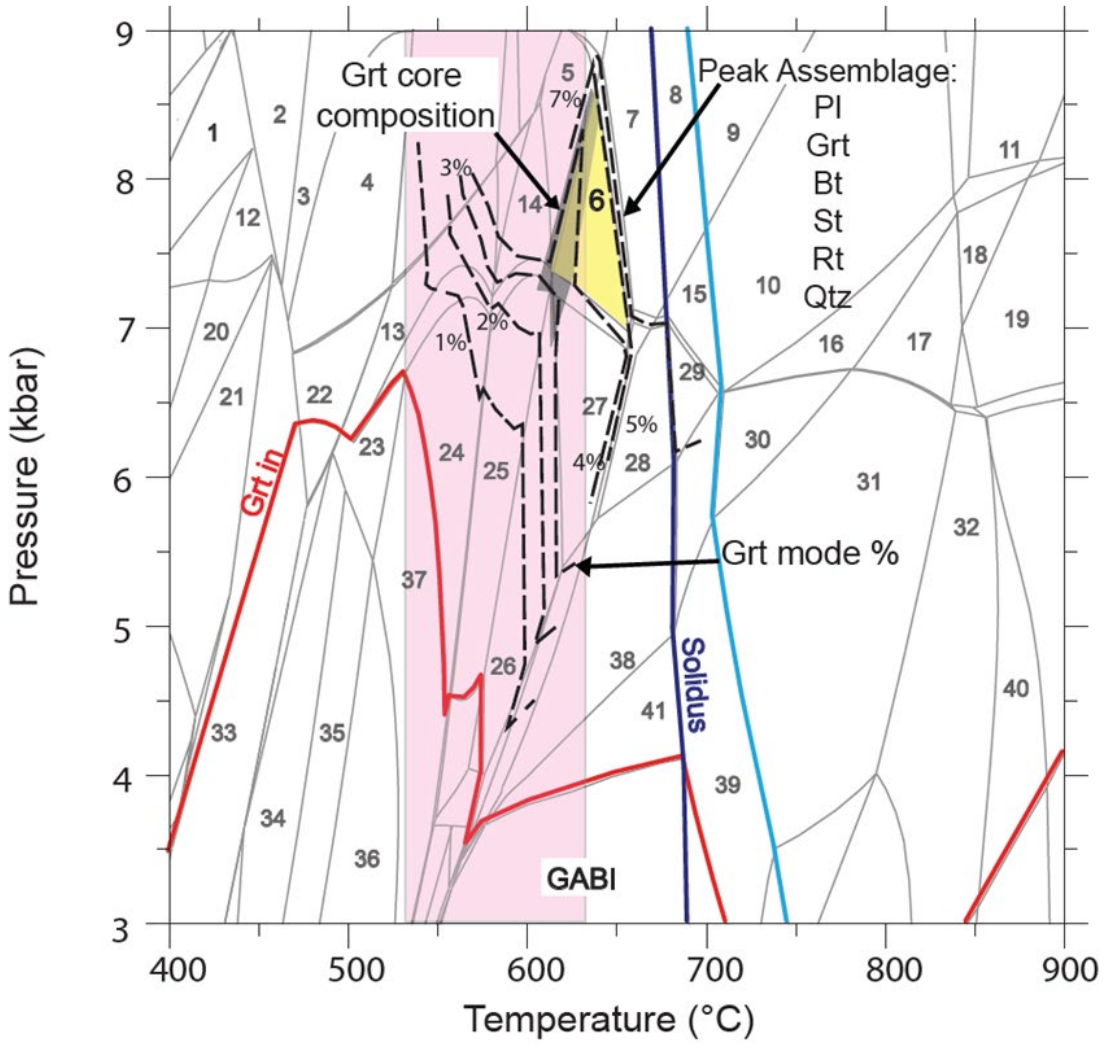

Figure 12. Simplified P-T mineral assemblage diagram for garnet-biotite schist, Sample 95AKEP06. The yellow polygon shows the predicted stability of the observed peak metamorphic mineral assemblage: garnet, staurolite, biotite, plagioclase, quartz, and rutile. The dark gray polygon indicates the area of intersection for predicted garnet end member isopleths for the observed garnet core composition. Dashed black lines indicate the predicted garnet volume percentage. The light pink rectangle indicates the P-T estimated garnet rim compositions based on GABI geothermometry. All assemblages are plus water. Appendix 1 summarizes the complete listing of predicted minerals.

EMB: Sample 19EBBC03

The following section describes the results from Sample 19EBBC03, the westernmost sample in the EMB.

Petrography

Sample 19EBBC03 is a garnet-biotite schist that was collected on a ridge east of Elbow Mountain in BC (Fig. 2), and multiple samples were collected from a large outcrop. Sample "A" was used for garnet geochronology because the garnet grains had slightly fewer inclusions. Sample "B" was used for P-T modeling and microprobe analysis because this rock is more similar to an average pelite; therefore, it is most appropriate for the activity models used in THERIAK-DOMINO (Table 3). 19EBBC03 is the westernmost sample from the EMB, within 25 km of the CSZ. This sample contains garnet, clinozoisite, chlorite, biotite, ilmenite, plagioclase, quartz, and opaques. Textural relationships indicate that the peak metamorphic mineral assemblage is garnet, clinozoisite, ilmenite, biotite, plagioclase and quartz. Chlorite is interpreted to be post peak assemblage because it was intergrown between the biotite grains. Garnet grains are ≤ 2.5 mm, anhedral, and poikioblastic. Inclusions in garnet include quartz and plagioclase, and these inclusions compose ~40% of the interior of the garnet grains. Most of the biotite occurs in ~0.5 mm layers that are interlayered with quartz-clinozoisite parallel to the mineral alignment. However, lesser amounts of biotite are mixed with the clinozoisite, quartz, and plagioclase layers (Fig. 13).

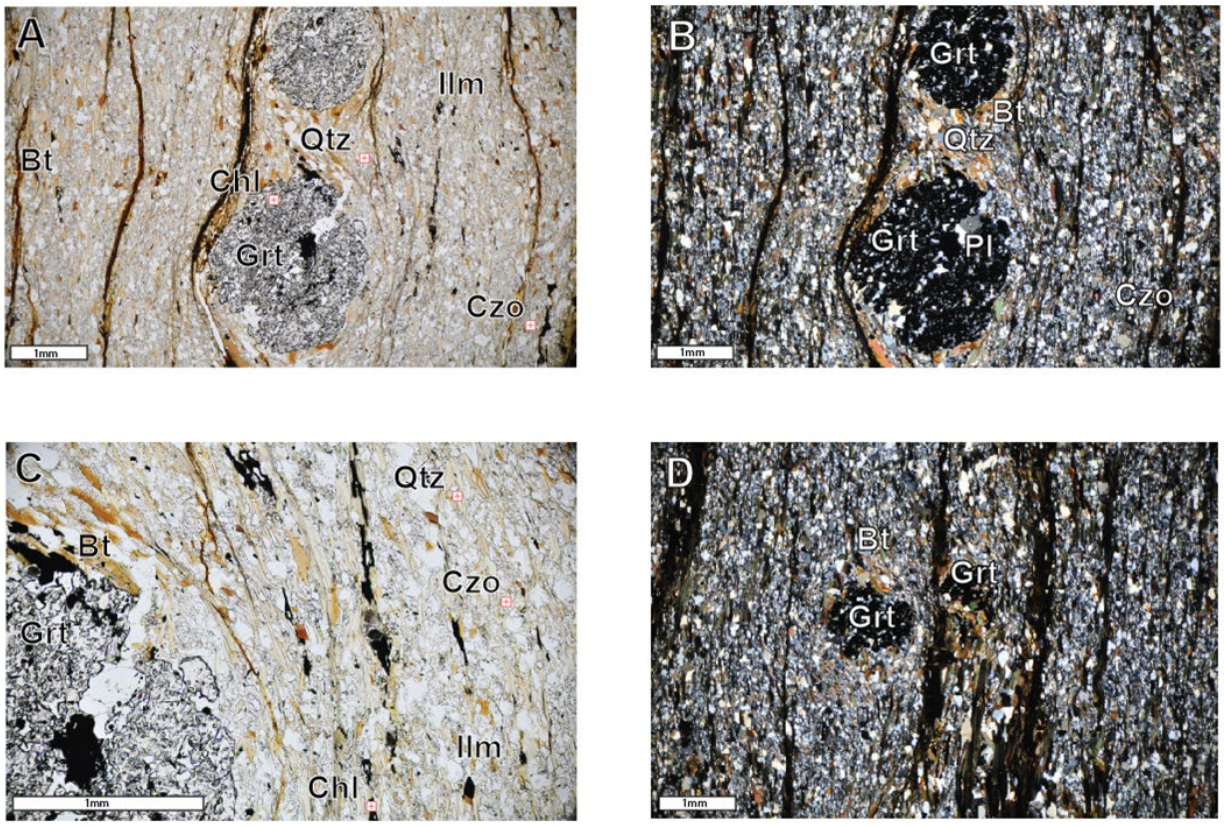

Figure 13. Photomicrographs of garnet-biotite schist, Sample 19EBBC03, from the EMB in BC. A) Plane polarized light image at 4x magnification and B) cross polarized light image 4x magnification showing garnet, clinozoisite, rutile, chlorite, biotite, and matrix material, including quartz and plagioclase. The large garnet grains are anhedral with numerous inclusions of plagioclase and quartz. Chlorite is interpreted to postdate deformation because it is overgrowing the matrix between the garnet rim and biotite layers. C) Plane polarized light image at 10x magnification of anhedral garnet rim with surrounding minerals and matrix. D) Cross polarized light image 4x magnification of anhedral garnet within matrix material and interspersed biotite layers. Garnet rims are heavily replaced by muscovite and biotite crossing the foliation, which are interpreted to postdate deformation.

Whole Rock Compositions

Sample 19EBBC03 is a pelite with high calcium compared to an average schist (Ague, 1991). Comparing the whole rock composition with average pelite compositions, Sample 19EBBC03B is higher in Fe_2O_3, MnO, and P_2O_5, is significantly higher in CaO (approximately 5%), is approximately equal in SiO_2 and TiO_2, and is lower in Al_2O_3, MgO, Na_2O, and K_2O. Table 3 summarizes the corresponding oxide concentrations for this sample.

Mineral Compositions

Garnet and biotite were analyzed from Sample 19EBBC03B. A ~2.3 mm garnet grain was analyzed to evaluate compositional zoning using EPMA point analysis across the grain. The abundant inclusions within the garnet grain made it difficult to collect quality garnet data at every increment; therefore, some analyses are extrapolated from nearby analysis points in place of those collected during the line scan. Additional point analyses were obtained for biotite and plagioclase to analyze any zoning and for GABI thermometry. Garnet end member zoning is as follows: $almandine_{core} = 0.62$ to $almandine_{rim} = 0.73$; $spessartine_{core} = 0.18$ to $spessartine_{rim} = 0.07$; $pyrope_{core} = 0.06$ to $pyrope_{rim} = 0.11$; and $grossular_{core} = 0.13$ to $grossular_{rim} = 0.08$. Major zoning fluctuations can be seen in Figure 14. Spessartine zoning follows a bell curve, where almandine, pyrope, and the magnesium number generally increase from core to rim. Grossular decreases from core to rim, with two pronounced "waves." Changes in zoning (e.g., slight increases in grossular, slight decreases in pyrope and magnesium number) are observed at ~0.1 mm from the rim. Tables 4-6 summarize the representative mineral analyses used for thermobarometry.

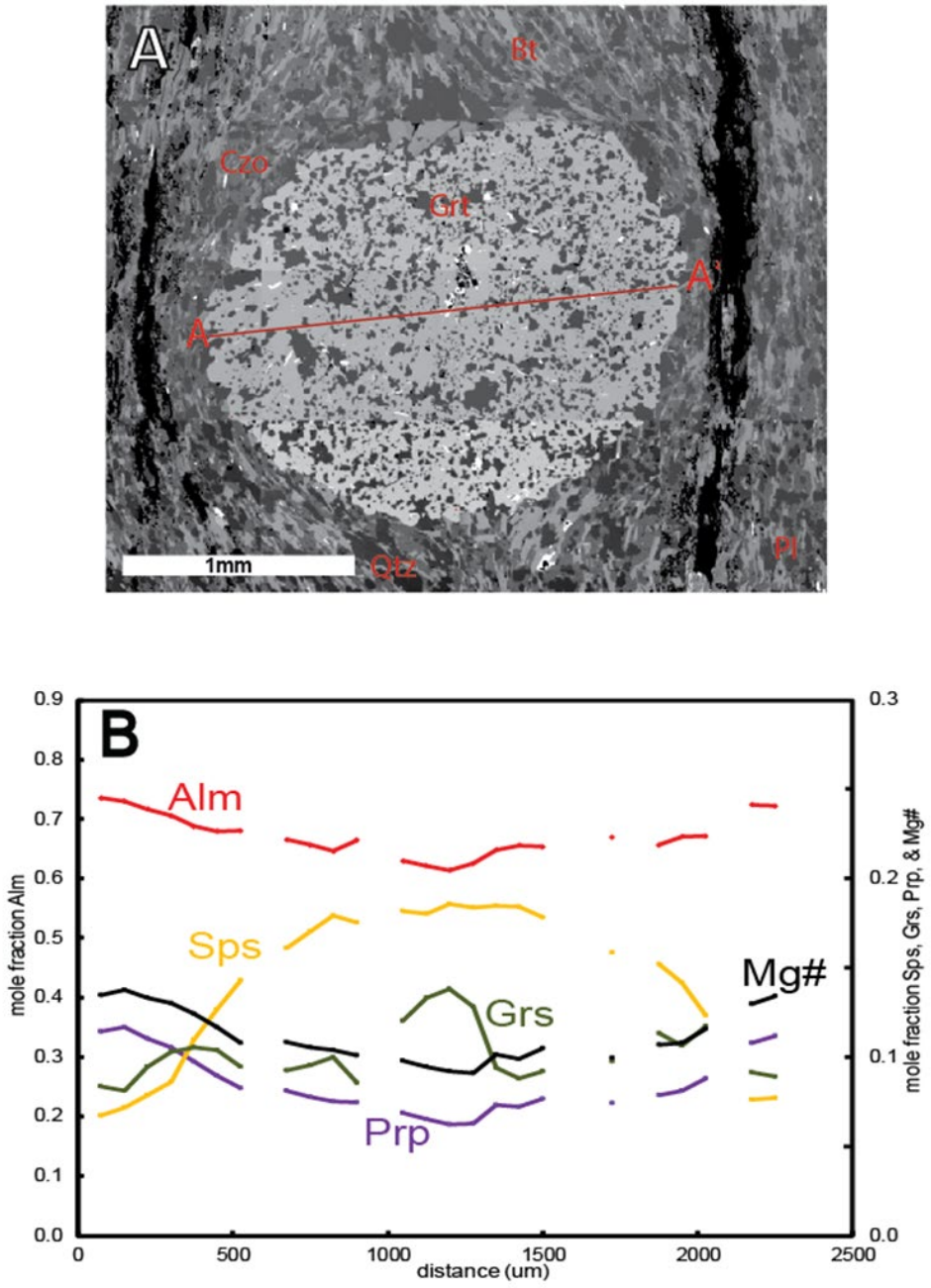

Figure 14. BSE map and compositional zoning profile for garnet in Sample 19EBBC03B. A) BSE image of garnet with profile A-A' indicating the line scan position. B) Garnet compositional zoning along profile A-A'. The line scan includes 52 WDS point analyses. Tables 4-6 summarize the full mineral analyses.

Garnet Sm-Nd Geochronology

Garnet Sm-Nd isochrons are constructed for Sample 19EBBC03A using four bulk garnet aliquots combined with matrix and whole rock aliquots. The garnet Sm-Nd age of metamorphism is 56.7 ± 0.7 Ma (2σ uncertainty) with an MSWD = 0.9. Sm and Nd isotope ratios and concentrations are summarized in Table 7. The low uncertainty and MSWD of ~1 indicate the simple garnet growth history in this sample.

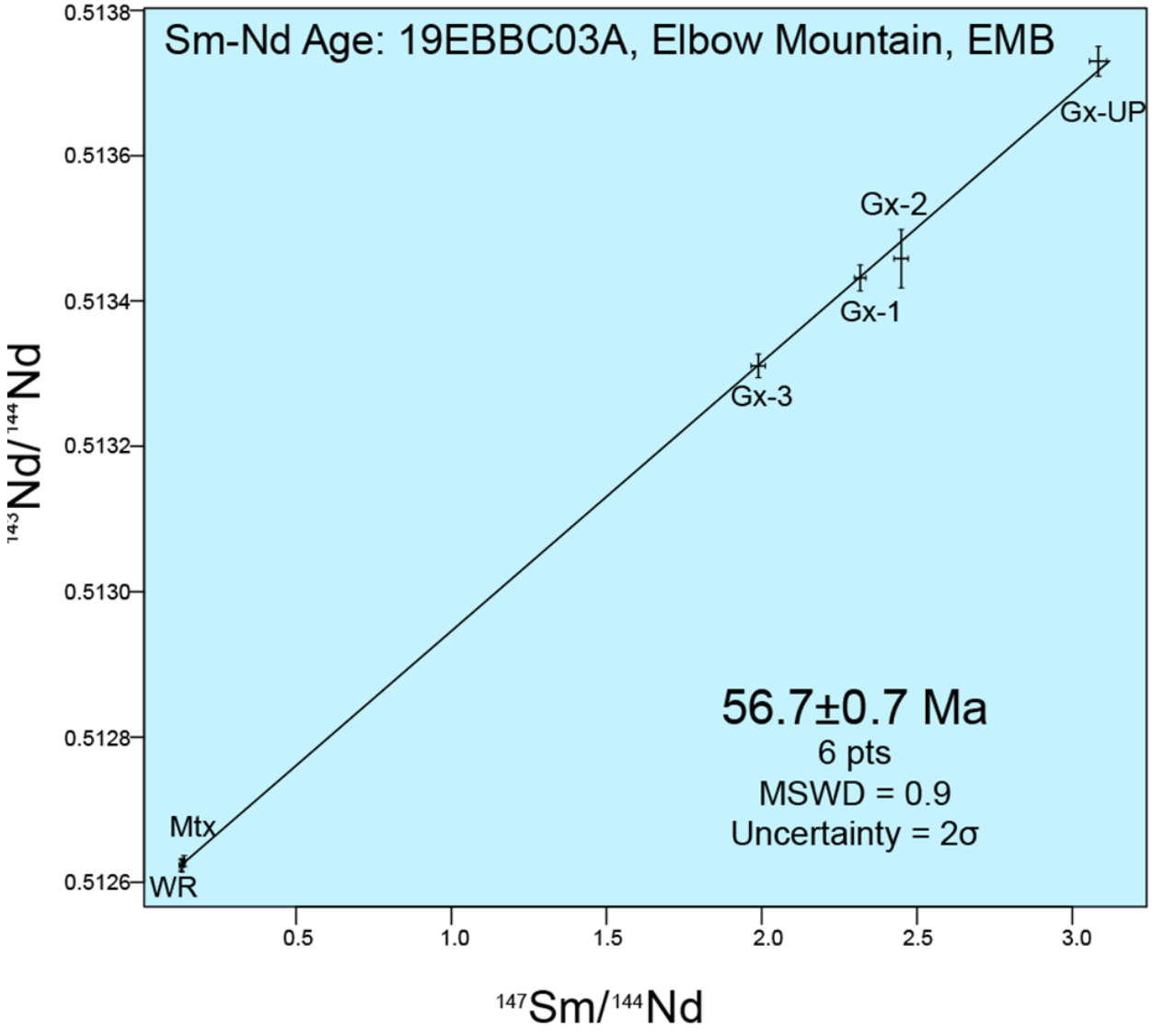

Figure 15. Sm-Nd isochron for garnet-biotite schist, Sample 19EBBC03. Isotope ratios for four garnet aliquots, matrix, and whole rock samples yield an age of 56.7 ± 0.7 Ma with an MSWD of 0.9. Age result and all isotope ratios are presented with 2σ uncertainties. Table 7 summarizes the associated isotope ratios.

P-T-t paths

The simplified P-T MAD for Sample 19EBBC03B is shown in Figure 16 and includes tentative pressure estimates. The peak mineral assemblage of garnet, clinozoisite, ilmenite, biotite, plagioclase and quartz observed in the rock does not plot in the P-T MAD. However, this assemblage plus margarite and chlorite plots as assemblage 19 on Figure 16. Given the lack of X-ray maps, it is possible that minor margarite is present in the sample. It is also possible that margarite is over predicted in the model. Another possibility to consider is that chlorite grew with the peak assemblage and may have been consumed by muscovite and/or margarite. By assuming that the rutile/ilmenite stability is independent of the white mica, staurolite, and aluminosilicates, the rutile/ilmenite line was used to constrain the maximum possible pressure. The lack of cordierite present in the sample constrains the minimum pressure as cordierite is present in assemblage 30 on figure 16. The combination of the garnet core P-T estimate, tentative maximum pressure limit, and the rim P-T estimate from geothermometry indicates a general P-T path that begins at ~550°C and 3.5-4.5 kbar and that peaks below 7 kbar. GABI geothermometry exchange reactions predict rim equilibration at 599 ± 50°C, which is indicated by the light pink rectangle in the Figure 16. This temperature estimate, combined with chlorite stability, is used to predict the end of the P-T path. Between the two, garnet volume percent is plotted as a black dashed line showing garnet growth between core and peak from 0 to 10%.

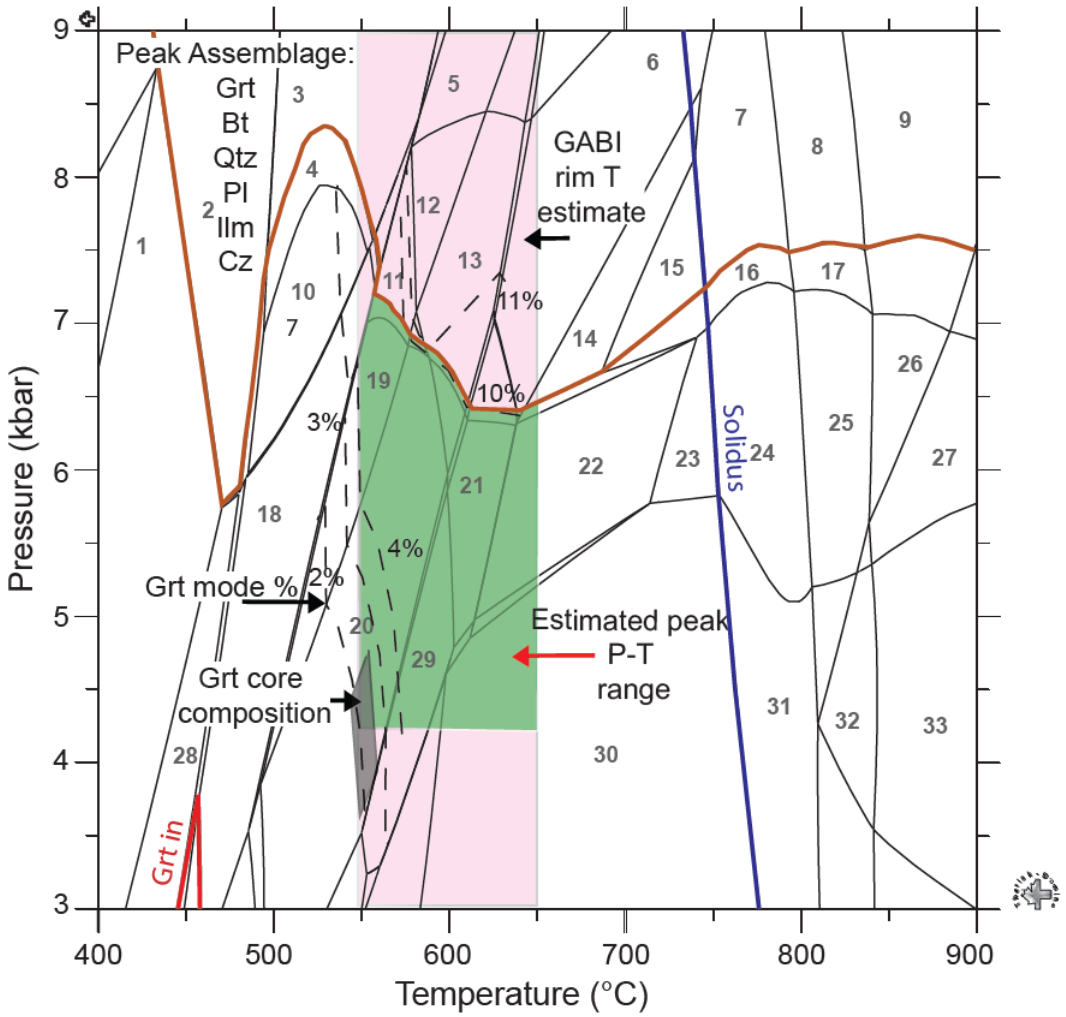

Major Mineral Stability Fields

3. Grt, Bt, Chl, (2) WM, Czo, Rt, Qtz **5.** Grt, Bt, WM, Mrg, Czo, Rt, Pl, Qtz
11. Grt, Bt, Chl, Rt, Czo, Mrg, Pl, Qtz **12.** Grt, Bt, Czo, Rt, Mrg, Pl, Qtz
13. Grt, Bt, Rt, Mrg, Pl, Qtz **19.** Grt, Bt, Chl, Czo, Ilm, Mrg, Pl, Qtz
20. Grt, Bt, Chl, Ilm, Mrg, Pl, Qtz

Figure 16. Simplified P-T mineral assemblage diagram for garnet-biotite schist, Sample 19EBBC03. The observed peak metamorphic mineral assemblage is garnet, biotite, clinozoisite, plagioclase, quartz, and ilmenite, but this assemblage is not observed on the MAD. The dark gray polygon indicates the area of intersection for predicted garnet end member isopleths for the observed garnet core composition. Dashed black lines indicate the predicted garnet volume percentage. The green polygon, called out by the red arrow, indicates the estimated peak P-T range. The dark orange line is the ilmenite-rutile line and is the maximum peak pressure estimate. The light pink rectangle indicates the P-T estimated garnet rim compositions based on GABI geothermometry. All assemblages are plus water. Appendix 1 summarizes the complete listing of predicted minerals.

EMB: Sample 19EBBC06

The following section describes the results from Sample 19EBBC06, the easternmost sample in the EMB.

Petrography

Sample 19EBBC06 was collected at the easternmost location in the study area, along the Stikine Transect, from the eastern flank of Elbow Mountain (Fig. 2), and this location is ~0.5 km east of the Sample 19EBBC03 collection site. Sample 19EBBC06 is subdivided into two samples: A, which is an in-place sample, and F, which is a float sample found on the large outcrop.

Sample 19EBBC06A is a garnet-biotite-schist, containing garnet, biotite, muscovite, pyroxene, plagioclase, quartz, and opaques. This sample differs from all other samples in that it contains veins of plagioclase and quartz that may be associated with a locally derived partial melt. The whole rock total Fe content is higher than average pelites and may have caused difficulties with the P-T models. Garnet grains are slightly larger and more prevalent in sample A; therefore, it was chosen for garnet geochronology. The garnet grain is ~2 mm in size, is anhedral, and includes plagioclase, quartz, and rutile needles. A small vein of chlorite and quartz runs through the garnet. Multiple veins exist within the sample, some of which are plagioclase and quartz dominant with chlorite present, and others that are biotite dominant. Biotite, quartz, and plagioclase are present as matrix material with not distinct foliation.

Sample 19EBBC06F is a garnet-biotite-andalusite schist that contains garnet, andalusite, sillimanite, plagioclase, quartz, rutile, and some opaques. It was collected approximately 10 m from Sample 19EBBC06A, but it was not an intact part of the outcrop. Index minerals including andalusite and sillimanite made this sample ideal for P-T and microprobe analysis. Large,

anhedral andalusite crystals are largely replaced with quartz and plagioclase. This, combined with sillimanite fibers growing along andalusite rims and around biotite grains, indicate the peak metamorphic assemblage to be garnet, sillimanite, rutile, biotite, plagioclase, and quartz. Garnet occurs as subhedral to anhedral crystals that are < 2 mm in size, with some containing inclusions of quartz and plagioclase. A few relict staurolite grains occur as anhedral grains that are largely replaced by muscovite, which crosscut the foliation. Schistosity is not well defined; however, the biotite is subtly aligned.

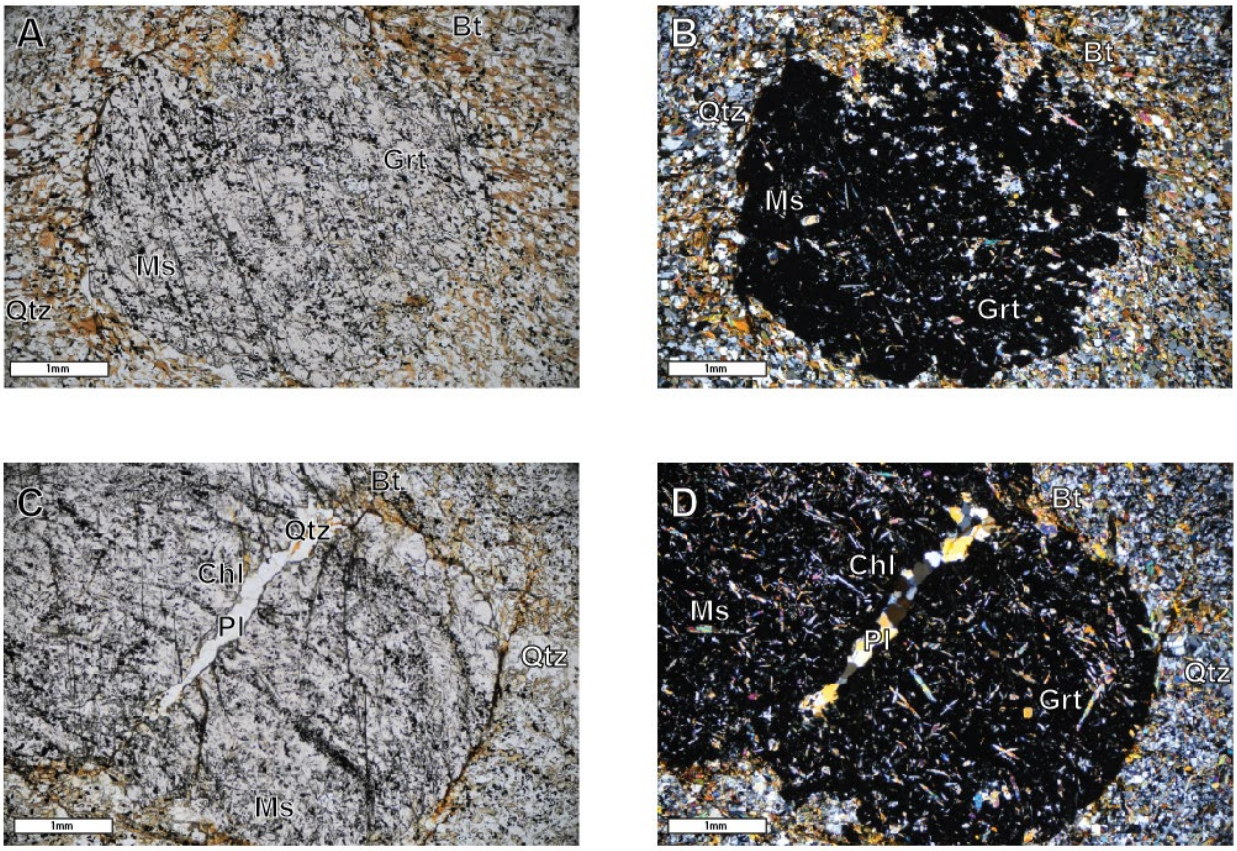

Figure 17. Photomicrographs of garnet-biotite schist, Sample 19EBBC06A, from the EMB in BC. A) Plane polarized light image and B) cross polarized light image showing garnet heavily included with muscovite and quartz and the adjacent matrix minerals. C) Plane polarized light image of two euhedral garnet grains that grew together, with major alteration replacing the adjacent rims with quartz, plagioclase, and some chlorite. D) Cross polarized light image of two euhedral garnet grains that grew together with major alteration replacing the adjacent rims and heavily included with muscovite.

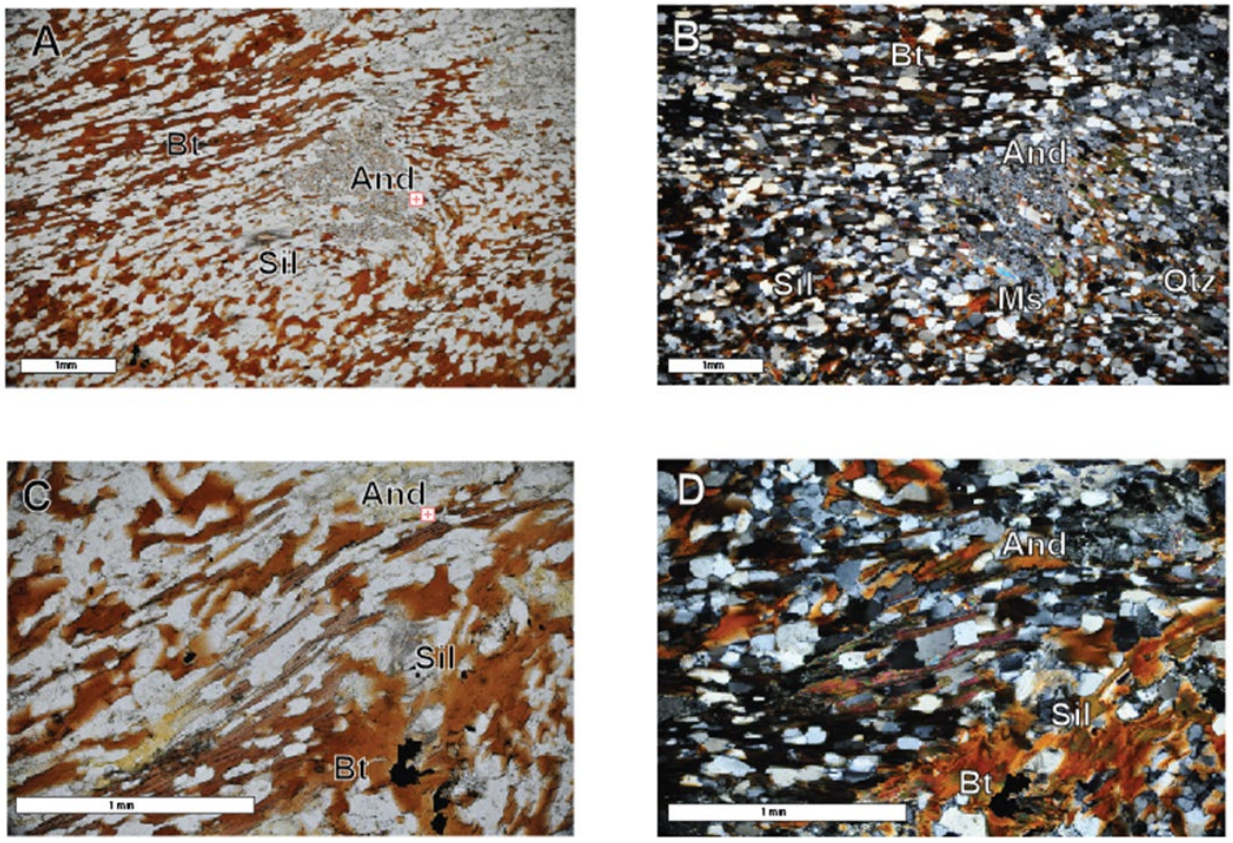

Figure 18. Photomicrographs of garnet-andalusite-sillimanite schist, Sample 19EBBC06F, from the EMB in BC. A) Plane polarized light image and B) cross polarized light image showing andalusite, sillimanite, and biotite with matrix minerals, including quartz and plagioclase. Large andalusite grains are heavily replaced with numerous inclusions of quartz and plagioclase. C) Plane polarized light image and D) cross polarized light image of andalusite, sillimanite, and biotite. Sillimanite appears as fibrolite adjacent to andalusite grains and around biotite grains. This is interpreted as early andalusite growth with sillimanite growth at peak metamorphic P-T.

Whole Rock Compositions

Samples 19EBBC06A and 19EBBC06F are pelitic schists with significantly different compositions considering their relative distance in the field. Comparing the whole rock compositions with average pelite compositions, Sample 19EBBC06F is higher in SiO_2, is approximately equal in CaO, Na_2O, and P_2O_5, and is lower in TiO_2, Al_2O_3, MnO, MgO, and K_2O. The presence of andalusite and sillimanite indicates it is a high aluminum pelite in terms of mineralogy (Ague, 1991; Spear, 1993); however, the aluminum silicate minerals were likely stabilized by low K_2O rather than high Al_2O_3. Table 3 summarizes the corresponding oxide concentrations.

Sample 19EBBC06A is anomalous compared to other samples collected along the transect (Fig. 2). Comparing the whole rock with average pelite compositions, Sample 19EBBC06A is significantly higher in Fe_2O_3, CaO, MgO, TiO_2, and Na_2O, is approximately equal in MnO, and is lower in SiO_2, Al_2O_3, and K_2O. This sample is considerably more mafic than other samples, with low SiO_2 and significantly higher Na_2O and CaO, compared to both average pelites (Ague, 1991) and to Sample 19EBBC06F.

Garnet Sm-Nd Geochronology

Sm and Nd isotope data for five bulk garnet aliquots, one garnet core aliquot, and a whole rock aliquot from Sample 19EBBC06A fail to plot in a single linear array. Instead, two poorly defined arrays suggest analytical problems or local disequilibrium; therefore, no meaningful isochron age can be calculated. The garnet aliquots plot almost equidistance above and below the calculated errorchron in two linear arrays. The garnet Sm-Nd age produced by this "errorchron" is 60.6 ± 28.7 Ma (2σ uncertainty) with an MSWD = 14 and is inconclusive. The two poorly defined, three-point data arrays may result from local disequilibrium and poor choices for the

garnet and whole rock aliquots. However, these arrays provide possible upper and lower age limits for garnet growth at ~73 Ma and 40 Ma (including 2σ age envelopes). Sm and Nd isotope ratios and concentrations are summarized in Table 7. Because of the low garnet mode and large amounts of inclusions in Sample 19EBBC06F, it was not chosen for garnet geochronology.

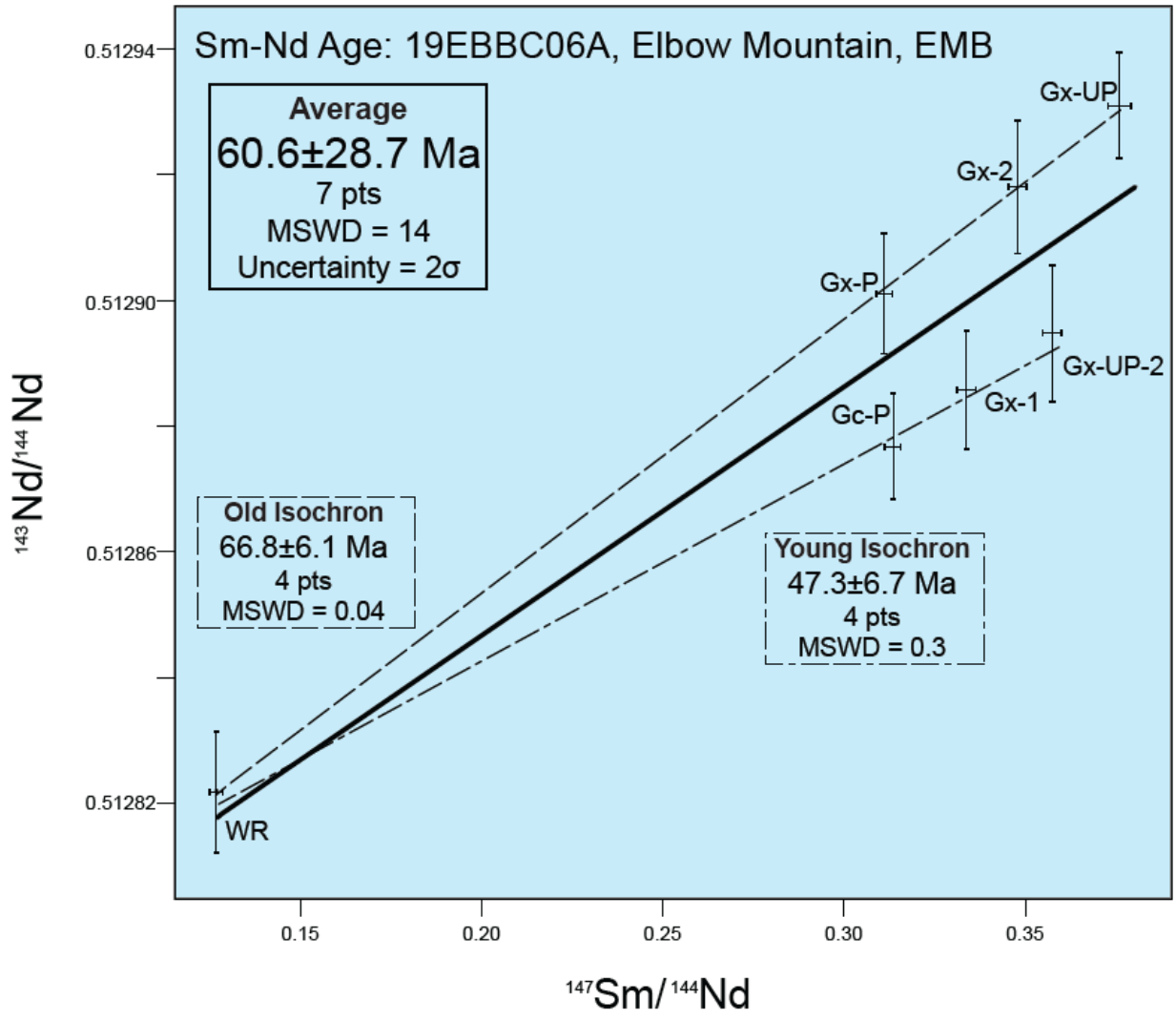

Figure 19. Sm-Nd data for garnet-biotite schist, Sample 19EBBC06A. Although the dataset results in an errochron, the two dashed lines may provide upper and lower limits for the garnet growth age.

P-T-t paths

The P-T MAD for Sample 19EBBC06F is shown in Figure 20. The observed mineral assemblages and replacement textures allow us to construct a P-T path. Heavily replaced andalusite indicates that early metamorphism is in the andalusite stability field, and prograde metamorphism reached peak metamorphic conditions in the sillimanite stability field. Garnet compositions are not available; therefore, compositional isopleths and rim thermobarometry are not completed for this sample. However, a P-T path can be inferred from the green outlined region of andalusite stability on the MAD (540 to 650°C below 4 kbar pressure) by extending along the red arrow to the peak metamorphic mineral assemblage, which is predicted at 600-700°C and 5-7 kbar.

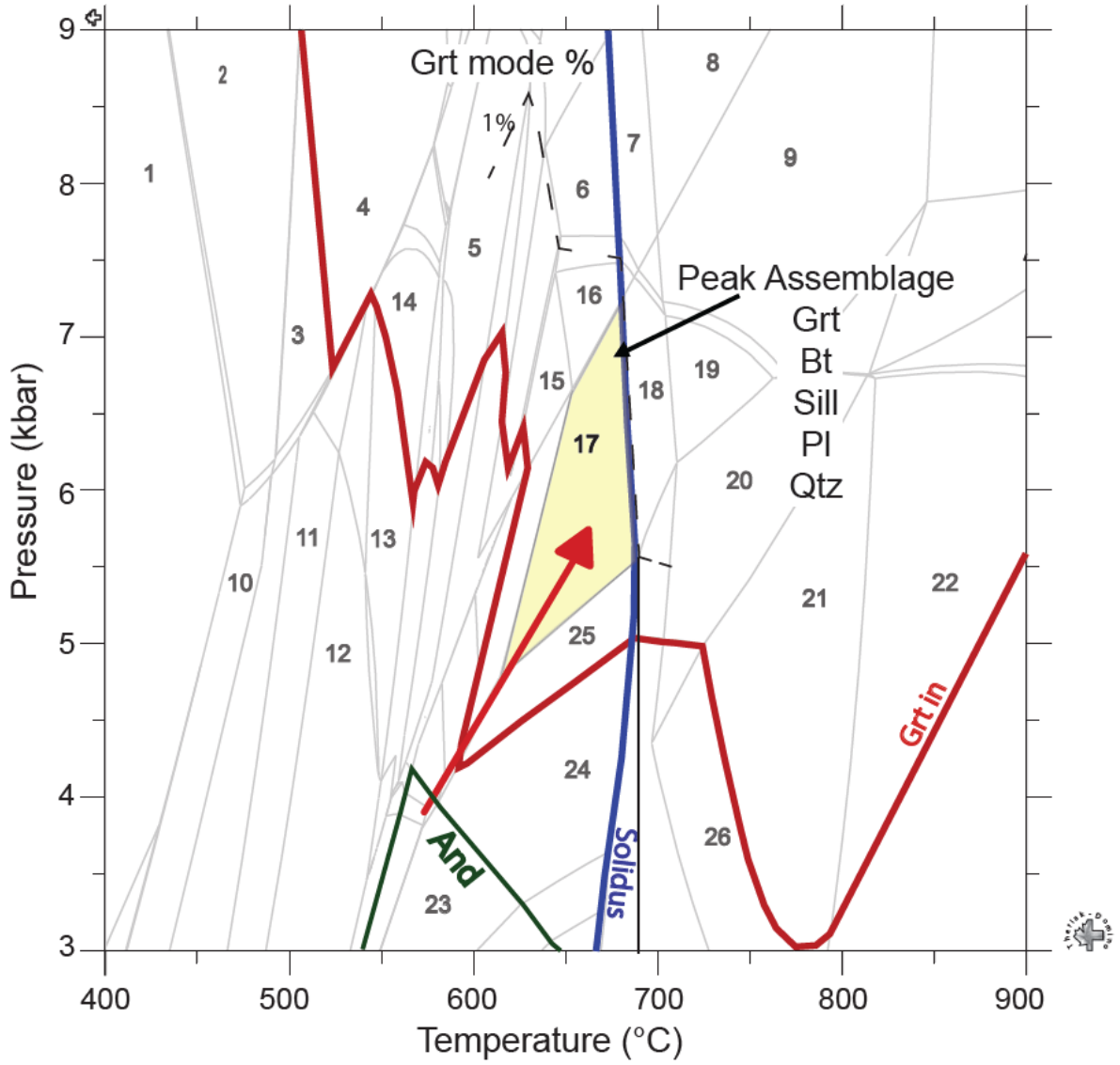

Major Mineral Stability Fields

15. Grt, Bt, St, Ky, Ilm, Pl, Qtz **16.** Grt, Bt, Ky, Ilm, Pl, Qtz
17. Grt, Bt, Sill, Ilm, Pl, Qtz **18.** Grt, Bt, Sill, Ilm, Pl, Qtz
23. Bt, And, Ilm, Crd, Pl, Qtz **25.** Grt, Bt, Sill, Ilm, Crd, Pl, Qtz

Figure 20. Simplified P-T mineral assemblage diagram for garnet-biotite schist, Sample 19EBBC06F. The yellow polygon shows the predicted stability of the observed peak metamorphic mineral assemblage: garnet, biotite, sillimanite, plagioclase, quartz, and rutile. Dashed black lines indicate the predicted garnet volume percentage. The dark gray polygon indicates andalusite stability and is interpreted to predate major deformation. The red arrow indicates the interpreted P-T path. All assemblages are plus water. Appendix 1 summarizes the complete list of predicted minerals.

DISCUSSION

Garnet Leaching

The garnet leaching procedures are well-tuned and generally follow those described by Gatewood et al. (2015); however, the time leached in 120°C HF was varied in this study. Hot HF acid is critical for dissolving silicate inclusions left within the crushed and picked garnet, but there is a classic tradeoff. While a longer HF leaching removes more inclusions, it also dissolves more garnet. A "clean" garnet (i.e., an inclusion-free garnet) should be recognizable on an isochron plot as the highest Sm/Nd ratio, relative to the other aliquots. This is demonstrated by Sample 19EBBC03, for which six aliquots define the isochron: two rock and four garnet. Of the four garnet aliquots, three were picked and leached for 60 minutes, and one was unpicked and leached for 80 minutes. The unpicked garnet aliquot has a significantly higher Sm/Nd than the picked aliquots, despite the greater mass of inclusions that must have been present in the unpicked sample (Fig. 15). All garnet aliquots have Sm/Nd ratios > 2.0; however, the intensely leached and unpicked garnet aliquot has a Sm/Nd ratio of almost 3.0. For Sample 95AKEP04, the isochron is made up of four garnet aliquots and two rock aliquots. Two of the garnet aliquots were leached in 120°C HF for 20 minutes, while the other two were leached for 40 minutes. The aliquots with shorter leaching times have Sm/Nd ratios of 0.23 and 0.31, where the aliquots with longer leaching times have Sm/Nd ratios of 0.42 and 0.51 (Fig. 7). The other samples analyzed display similar patterns. Aside from the 120°C HF leaching time, all other procedures are identical for all aliquots.

Ultimately, a cleaner garnet and a higher Sm/Nd ratio lead to a more precise isochron age, and longer HF leaching is the most efficient means to higher Sm/Nd ratios. This leads us to conclude that the cleanest garnet and best garnet Sm-Nd age results require a relatively high garnet mass and long HF leaching time.

Timing, Pressure and Temperatures of Metamorphism

Most garnet in the metamorphic rocks from the WMB and the EMB are interpreted to preserve major element and REE compositions that are useful for constructing prograde metamorphic histories across the CMB. However, Sample 95AKEP06 has decreasing pyrope and magnesium number from core to rim that are compatible with some modification of zoning. The following discussion of major element zoning in garnet from each examined sample along the Stikine transect (Fig. 22) provides the rationale for this interpretation.

Garnet zoning in the WMB. Garnet from the WMB samples (95AKEP04 and 95AKEP06) preserve significant prograde growth zoning. This assessment is based on bell-shaped manganese zoning patterns, with narrow (< 250 um) inflections in zoning at the rims, indicating some late modification and core compositions that generally predict lower pressure and temperature than those of the peak metamorphic assemblage. The bell-shaped Mn zoning across the garnet is typical of growth zoning that reflects fractionation of Mn into garnet and depletion of available manganese in the rock (Hollister, 1966). However, Sample 95AKEP06 has iron and magnesium zoning compatible with late modification of the major elements discussed above, and this could account for the slightly younger age of 0.4 – 17.2 Ma, considering uncertainties, for Sample 95AKEP06.

The prograde metamorphic path of Sample 95AKEP04 has a peak at 640-670°C and at 7-9 kbar, based on the predicted peak mineral assemblage shown in the Figure 8. Iron and

magnesium concentrations and the magnesium number should reach their maximum values at the peak temperature. Minute downticks in the magnesium content and the magnesium number at the very edge of the garnet rims indicate that some diffusion modified the outer 150 ɥm of the grains. However, with a lack of a measurable increase in Mn at the rim, little to no garnet consumption is inferred. Therefore, the values used for thermobarometry rim estimates were chosen from the point analysis with the highest pyrope and magnesium numbers, approximately 150 ɥm inside the rim. These estimates are ~0.5 kbar less than the peak assemblage pressure estimates. This is attributed to near isothermal garnet rim equilibration during unloading, and this interpretation is supported by the subparallel P-T path and garnet modes.

The prograde growth path inferred for Sample 95AKEP06 is similar to that of Sample 95AKEP04 but with half the P-T range. Garnet core growth, the peak metamorphic assemblage, rim thermometry, and late mineral growth all overlap on the P-T MAD in Figure 12 from 6.8-8.5 kbar. No pressure variations are required from the thermodynamic modelling nor from the observed grossular zoning. Staurolite stability is predicted after initial garnet growth, and inflections in garnet modes indicate that it could account for some garnet consumption near 625°C. The peak metamorphic field indicates garnet grew during increasing temperature and pressure, at approximately 7.5 ± 1 kbar and 600-650°C. Although no pressure estimates are possible, the GABI geothermometer indicates rim conditions of 540-640°C. The overlap of estimated P-T conditions is compatible with some modification of garnet zoning after growth.

The major element zoning described above indicates limited to no intracrystalline diffusion of major elements in garnet. Experimental work indicates that the REE diffuse at significantly slower rates than major elements (Carlson, 2006; 2012). Therefore, despite the lack of trace element concentrations and zoning for garnet, it is inferred that the REE have not been

significantly modified by diffusion. With this assumption, the garnet Sm-Nd ages from the WMB, based on whole garnet aliquots, indicate an integrated age for the prograde metamorphic path between 95 and 87 Ma. Some or all of the garnet growth may have been driven by plutonism, as described for Garnet Ledge (Stowell et al., 2001).

Garnet zoning in the EMB. Garnet zoning is only available from one sample from the EMB: Sample 19EBBC03B. The zoning is somewhat more complex than that described for the WMB samples. Grossular zoning is the most complex, with a high Ca core, a decrease toward the rim, and at least one additional peak in Ca between the core and rim. The zoning is interpreted as prograde within the garnet core, with modification and possible diffusion near the rims. Rim modification is identifiable by the reversal in pyrope content and the magnesium number in the garnet zoning profile (Fig. 14) and is interpreted to result from garnet consumption during late chlorite growth and cooling. Fluctuations of grossular and smaller changes in almandine may reflect whole rock metasomatism during garnet growth. Because the preserved spessartine zoning is simple in the core, it is assumed that the garnet core P-T estimate is valid.

P-T-t paths: P-T-t paths along the Stikine transect indicate dramatic differences in the timing of garnet growth and the loading history across the CMB. These P-T-t paths are anchored by the new garnet Sm-Nd ages presented in this thesis, which are the first direct dates for garnet growth across the CMB in the Stikine area. The two garnet ages from the WMB indicate that regional metamorphism in the WMB occurred between ~95 and 87 Ma. The main difference between the WMB samples is the narrower P-T range in Sample 95AKEP06, only 1.8 kbar, compared to the MAD P-T range of 3 kbar for Sample 95AKEP04 (both considering maximum uncertainties). This difference is determined from garnet core isopleths, rim thermobarometry, and thermometry, and it could indicate slightly earlier garnet growth in Sample 95AKEP04. Garnet

growth in Sample 95AKEP06 would have been late, relative, and occurred during the pressure increase. This conclusion is further supported by the slightly older garnet Sm-Nd age, 0.4-17.2 Ma, considering uncertainties, for Sample 95AKEP04, which preserved more of the pressure increase during loading. Another possible explanation for the difference between the WMB samples is insufficient microprobe analysis of Sample 95AKEP06, which may have missed slight changes in zoning along the core and rim. It is expected that a combination of these scenarios accurately explains the narrow pressure range, ~1.8 kbar, of Sample 95AKEP06.

These results correlate with the M2 and M3 metamorphic events described by Stowell and Tinkham (2003) and with the M2C and M2R events listed in Table 1. The M2R regional metamorphic event is tied to crustal thickening between 90-100 Ma (Stowell & Tinkham, 2003), which likely produced the pressures necessary for kyanite stability in Sample 95AKEP04. This event was closely followed by a post 90 Ma contact metamorphic event that emplaced tonalite plutons, corresponding with Garnet Ledge (Stowell et al. 2001), which is approximately 25 km from where the WMB samples were collected (Figs. 2; 21). Generally, the P-T paths and ages from the WMB samples are similar. Core garnet growth occurred around 600°C and 6-7.75 kbar and peaked at 600-700°C and 7-9 kbar. The garnet age of metamorphism is interpreted to reflect the increasing pressure and temperature part of the P-T path during core garnet growth at ~87-95 Ma. These paths end at 550-700°C and 4.5-6.5 kbar, and this pressure decrease is likely representative of the early stages of unloading in the WMB.

Metamorphism of rocks in the EMB is more difficult to interpret than for those in the WMB due to limited data, MAD limitations for Sample 19EBBC03B, and relatively complex garnet zoning. The P-T MAD for Sample 19EBBC03B does not predict the exact peak mineral assemblage observed in the rock. While the P-T model was run with several variations, none of

the results predicted the observed minerals. Given this, the rutile mode zero line, which remains near constant in all model runs, was used to interpret an approximate maximum pressure. The upper limit is predicted at 6.5-7 kbar, based on the occurrence of ilmenite and the lack of rutile in the rock. Two possible scenarios may have caused the discrepancies in predicting the peak mineral assemblage. First, the garnet Sm-Nd age for this sample may represent the high temperature resetting by REE diffusion. In this case, the age of 57 ± 0.7 Ma would date a high temperature thermal event after initial garnet growth. Alternatively, metasomatism, probably from a flux of fluid moving through the rock, may have effectively altered the whole rock composition. The second scenario may be more likely because metasomatism would also explain the abundant clinozoisite present in the rock, which is locally replacing early plagioclase. Most of the remaining plagioclase occurs as garnet inclusions, and the remainder is in the matrix. Considering that garnet in this sample preserves manganese growth zoning, and that grossular and almandine fluctuate with increases towards the rim, an influx of Fe- and Ca-bearing fluids into the rock may have occurred as the garnet grew.

The P-T- path for Sample 19EBBC03B is interpreted to begin with garnet core growth at ~550°C and 3.5-4.5 kbar, continuing to peak at ~600°C and 6.5-7 kbar, which is below the ilmenite to rutile transition. This path is supported by the MAD predictions for increased garnet mode as well as by the GABI geothermometry, which indicates garnet rim equilibration at 550-650°C. Garnet core composition constrains the low temperature limit for peak garnet growth, while predicted mineral assemblages, including staurolite and aluminum silicates, neither of which occur in this rock (Fig. 16), constrain the upper temperature limit. Therefore, peak garnet growth must not have occurred outside this temperature range. These results indicate the age of 57 ± 0.7 Ma represents the garnet core growth to peak metamorphic time in the P-T path.

Metamorphic rocks collected further east of Sample 19EBBC03 (e.g., Sample 19EBBC06) preserve sillimanite replacing andalusite, which constrains the P-T conditions of initial garnet growth to pressures below the aluminum-silicate triple point at 4.5 kbar and 530°C (Holland & Powell, 2011). The P-T path increases in pressure and temperature into the sillimanite field to the predicted peak metamorphic mineral field (Fig. 20) at 5-7 kbar and 600-700°C. This implies that at least some of the eastern CMB experienced ~1 kbar loading during garnet growth.

The results confirm that garnet growth and most metamorphism in the EMB is ~30 million years younger than that in the WMB. Along with kyanite stability, P-T modeling indicates a ~3 kbar difference in peak metamorphic pressures on either side of the CMB. This result indicates at least 10 km of exhumation in the WMB. The WMB rocks do not show signs of alternation after garnet growth, dated at ~90 Ma, and therefore must have been exhumed considerably earlier than exhumation in the WMB. Approximately half of the significantly greater exhumation in the WMB occurred between 95 and 60 Ma, based on pressures for metamorphism of ~8 kbar adjacent to the 95 Ma diorite pluton at Garnet Ledge and the 60 Ma tonalite sill plutons that experienced pressures upwards of 9 kbar that are found ~150 km further north (Stowell & Goldberg, 1997). Although no data are available for the central CMB on the Stikine transect, it is speculated that much of this difference in pressure and exhumation may be focused across the CSZ.

Plutonism, Metamorphism and Tectonic Models

The Coast Mountains are the eroded roots of a magmatic arc with a long history of magmatic pulses (e.g., van der Hayden, 1992; Gehrels et al., 2009). New zircon U-Pb ages from the Stikine transect provide insight into the plutonic history of the batholith (Cecil, unpublished). Most of the new age constraints, which were obtained for samples collected near the merger of the

Stikine and Iskut Rivers, are between 50 to 60 Ma, and near 85 Ma (Fig. 21). Further east, the plutons are older. For example, a pluton located at 56.703056°N and 131.864722°W, has an age of 161 Ma, and another pluton located ~10 km further east has an age of 194 Ma. These plutons are clearly from an earlier magmatic event, which emplaced them into the Stikine and Yukon-Tanana terranes (Fig. 2). The new garnet Sm-Nd ages in this thesis help to constrain the importance of regional contact metamorphism versus metamorphism resulting from crustal thickening and thermal relaxation across the Coast Mountains.

Magmatic pulses can heat significant areas within the middle to upper crust and are likely sources of regional contact metamorphism in magmatic arcs (e.g., Barton et al., 1988). By combining zircon U-Pb ages from plutons with the metamorphic garnet Sm-Nd ages derived in the current study, we can potentially link specific metamorphic events to magmatic activity. Three well defined plutonic events were defined by Gehrels et al. (2009). First, a magmatic event in the Alexander and Wrangellia terranes was active over three phases from 177-100 Ma. Second, in the Stikine and Yukon-Tanana terranes, an active pulse occurred between 180-110 Ma. Finally, a major pluton emplacement event occurred from 100-50 Ma, which migrated from west to east across multiple terranes and what is now the central batholith. Stowell et al. (2001) link garnet growth in the Wrangell /Garnet Ledge area to emplacement of the Cretaceous quartz diorite pluton at Garnet Ledge, which is interpreted by some to underlie a large part of the WMB west of the Stikine River estuary. The pluton at Garnet Ledge has a zircon U-Pb age of 91.6 ± 0.5 Ma (Stowell et al., 2001) and a garnet Sm-Nd age of 89.9 ± 3.6 Ma, indicating part of the third magmatic event described by Gehrels et al. (2009). Garnet Sm-Nd ages reported here for Samples 95AKEP04 and 95AKEP06, which were collected ~25 km SE of Garnet Ledge, range from 95 to 87 Ma; therefore, a ~90 Ma regional event is inferred. However, the emplacement of

the plutons responsible for metamorphism at Garnet Ledge may have caused regional heating, in addition to thermal relaxation after loading from Cretaceous thrusts faults.

The younger zircon U-Pb ages from the central CMB (McClelland et al., 2000; Cecil, unpublished) indicate emplacement of numerous plutons east of the CSZ at ~55 Ma. This magmatic pulse may have provided at least some of the heat causing metamorphism in this area. In the case of Sample 19EBBC03, there are ~60 Ma plutons located within 10 km of the sampling location (Fig. 21). Therefore, regional contact metamorphism may have affected the EMB in a similar manner to the WMB but ~30 million years later.

The Skeena fold and thrust belt, located ~200 km south of the Stikine River, is a complex regional-scale structure of Jurassic – Mid-Cretaceous age (Evenchick et al., 2007). Similar to the Elbow Mountain area, deformation and plutonism dating to ~50 Ma has been documented. This indicates that the EMB and areas further east of the northern Coast Mountains, near the Stikine/Iskut River region, could have similar structure and timing to the Skeena fold and thrust belt; however, more structural data is needed to confirm this hypothesis.

New garnet Sm-Nd ages and published ages for the WMB establish that metamorphism in the EMB is significantly younger than in the WMB. WMB garnet Sm-Nd ages range from 95 ± 5 Ma to 87 ± 4 Ma (2σ), while those in the EMB are 57 ± 1 Ma (2σ). Garnet growth on both sides of the batholith occurred during loading; however, the pressure increase in the EMB may have been negligible (≤1 kbar). The WMB was loaded ~95 Ma, and the EMB rocks were loaded ~57 Ma, likely syn to post exhumation of the WMB. McClelland et al. (1991) describe uplift of the eastern portion of the WMB, accompanied by Late Cretaceous to Paleocene emplacement of foliated tonalite sill plutons. The new garnet ages for the EMB provided in this thesis confirm

that metamorphism and pluton emplacement in the east is ~30 million years younger than that in the west.

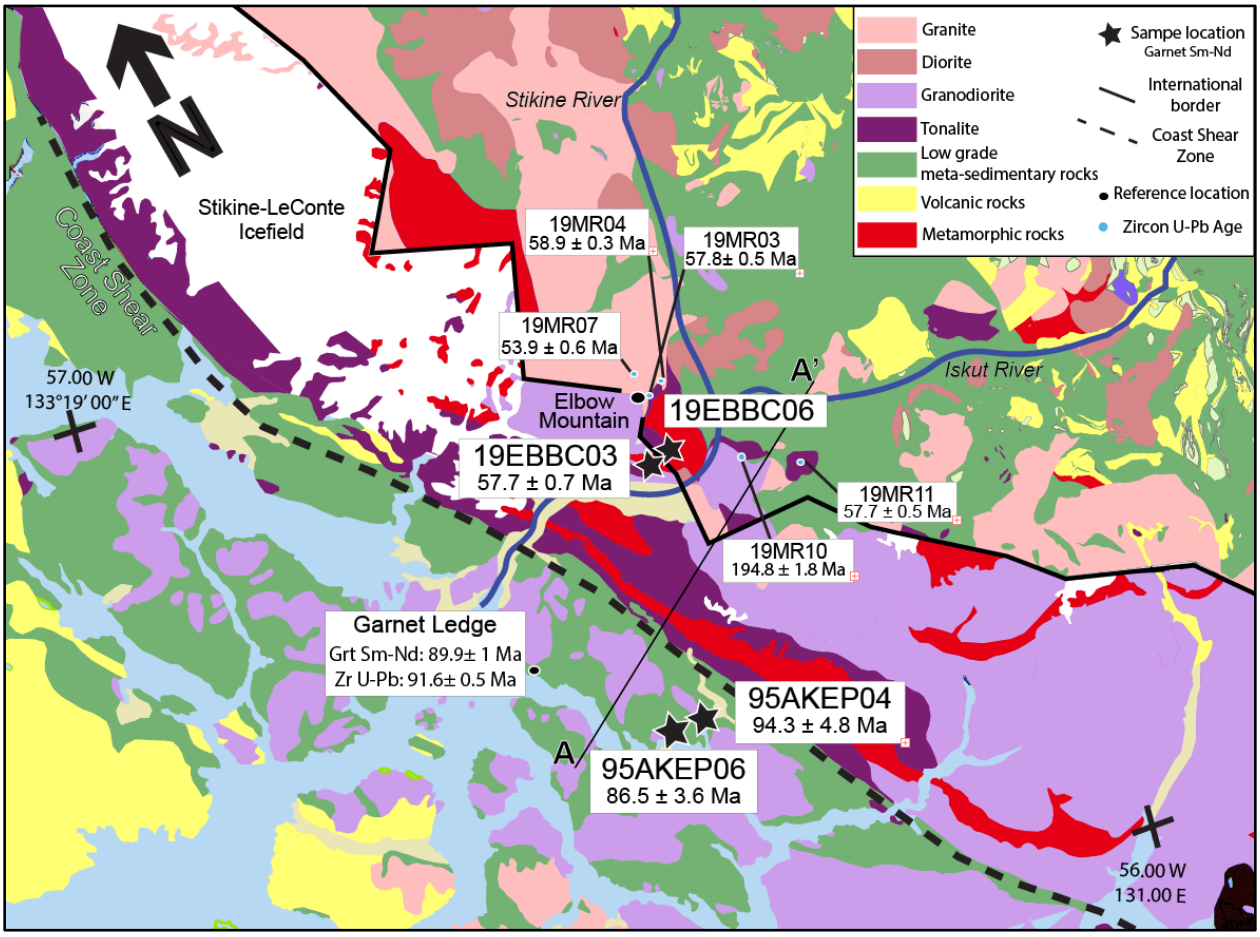

Figure 21. Simplified geologic map of the CMB, the WMB, and the EMB in the Stikine River area of southeast Alaska and adjacent BC. This map shows the general distribution of rocks, garnet Sm-Nd ages from Garnet Ledge (Stowell et al., 2001) and samples from this thesis, and zircon U-Pb (Cecil, unpublished) ages near the Stikine River. Modified from Gehrels & Berg (1982) and Cui et al. (2017).

The uplift and exhumation of the WMB was likely much earlier than that of the central batholith and EMB, based on $^{40}Ar/^{39}Ar$ cooling ages for the tonalite sill near Holkham Bay to the north (Wood et al., 1991; Stowell & Pike, 2000) and K-Ar ages near the Stikine River transect (Aleksey, 2021). Although the exact timing of uplift and exhumation is unknown in the WMB, the following provide some constraints. Garnet growth at ~95 Ma has not been documented anywhere in the EMB nor in the central batholith; however, in the CGC metamorphism has been interpreted to pre-date dikes with zircon U-Pb ages of ~80 Ma. (Pearson et al., 2017). The estimated metamorphic pressure of ~8 kbar for WMB samples requires a burial depth of ~24 km. While the average geothermal gradient in the Earth's crust is 20-25°C/km, temperatures may have been > 30-35°C/km in this area of high magmatism (e.g., Barton et al., 1988). In this case, the WMB rocks would have attained an equilibrium temperature of 480-720°C, within the range of the presented temperature estimates. Cook and Crawford (1994) present $^{40}Ar/^{39}Ar$ biotite (Bt) and hornblende (Hbl) cooling ages across the WMB about 20 km north of Ketchikan, which range from 74-89 Ma, decreasing towards the CSZ and the central batholith. Aleksey (2020) compiles $^{40}Ar/^{39}Ar$ and K-Ar of Hbl and Bt cooling ages, and they indicate 80-95 Ma cooling ages near Wrangell in the WMB, with a sharp decrease in cooling ages along the WMB-CSZ contact. The Hbl cooling ages adjacent to the CSZ are 54 to 49 Ma, likely resulting from Paleocene east-side-up displacement across the CSZ and intrusion of ~60 Ma plutons in the central batholith. These data confirm that cooling and likely exhumation in the WMB began early relative to that in the central CMB and the EMB.

The timing and nature of metamorphism in the central CMB is poorly constrained in the Stikine River area; however, ~200 km south, the CGC was metamorphosed at ~10 kbar at ~90 Ma (Rusmore et al., 2005). The CGC was rapidly exhumed between 90 and 52 Ma (Rusmore et

al., 2005). The following tectonic scenarios for the Stikine River area incorporate this CGC history near the Skeena River (Fig. 2).

Two broad scenarios are considered to explain the data. The central batholith, east of the CSZ, was buried at depth with the WMB, and it experienced high pressure, similar to that in the WMB. This scenario is documented in the CGC along the Skeena River to the south (Hollister & Andronicos, date). Alternatively, the central batholith may never have experienced the 8+ kbar pressures documented in the WMB. In this scenario, the central batholith and EMB may have been separated from the WMB by a fault, possibly the CSZ. Before considering any further specifics, its important to note that numerous authors (McClelland et al. 1992) have interpreted strike-slip motion along the CSZ; however, the tectonic models presented here are based solely on temperature, pressure and/or depth and therefore cannot constrain strike-slip motion along the CSZ

After considering the two broad scenarios noted above for the structural framework of the Coast Mountains, three detailed scenarios are possible, given that the WMB was exhumed earlier than the EMB. First, the easternmost part of the WMB, the central CMB, and the EMB could have tilted as a coherent crustal block, with ~10 km more uplift on the west side, post 95 Ma. This scenario would require a continuous ‘smooth’ pressure gradient with the highest pressures on the west side. In addition, regional cooling ages would only reflect a ‘smooth’ gradient or disturbance by magmatic heating. Second, all or most of the WMB exhumation was accommodated by tilting of the WMB, with upward displacement of the highest temperature eastern WMB during mid-Cretaceous times. In this case, the central batholith in the Stikine area may not have experienced the high pressures observed in the CGC further south, and younger ages east of the CSZ could result from later heating without significant uplift. This scenario

would produce a sharp break in pressures at the CSZ. Third, the WMB was part of an orogenic wedge with westward directed faults up to ~95 Ma or shortly thereafter. In this case, the maximum crustal thickening and exhumation may have occurred in the eastern part of the WMB or in the central batholith. This concept is supported by the west-to-east increasing metamorphic grade in the WMB (McClelland et al., 1990; Stowell & Hooper 1990; Stowell et al., 1989). In this case, at least some displacement on the CSZ would be related to east-side-up displacement, and the central batholith would have reached conditions similar to those in the CGC further south. Early displacement on the CSZ could have been west-side-up during development of the orogenic wedge, switching to east-side-up displacement at ~55 Ma (Cook & Crawford, 1994), contemporaneous with late heating from Paleocene plutons that resulted in later cooling of the central batholith. The central CMB would have been exhumed from the high pressures post 60 Ma, and a pressure discontinuity between the central CMB and the EMB could result from west-side-up tilting. In addition, a detachment similar to the east side detachment in the Skeena River area could have accommodated unroofing. If the CSZ was associated with the orogenic wedge, then the CSZ may have accommodated reverse (west-side-up) displacement throughout much of its history (e.g., Stowell & Hooper, 1990). New data on the P-T history of the central batholith in the Stikine area is needed to test and differentiate between these ideas.

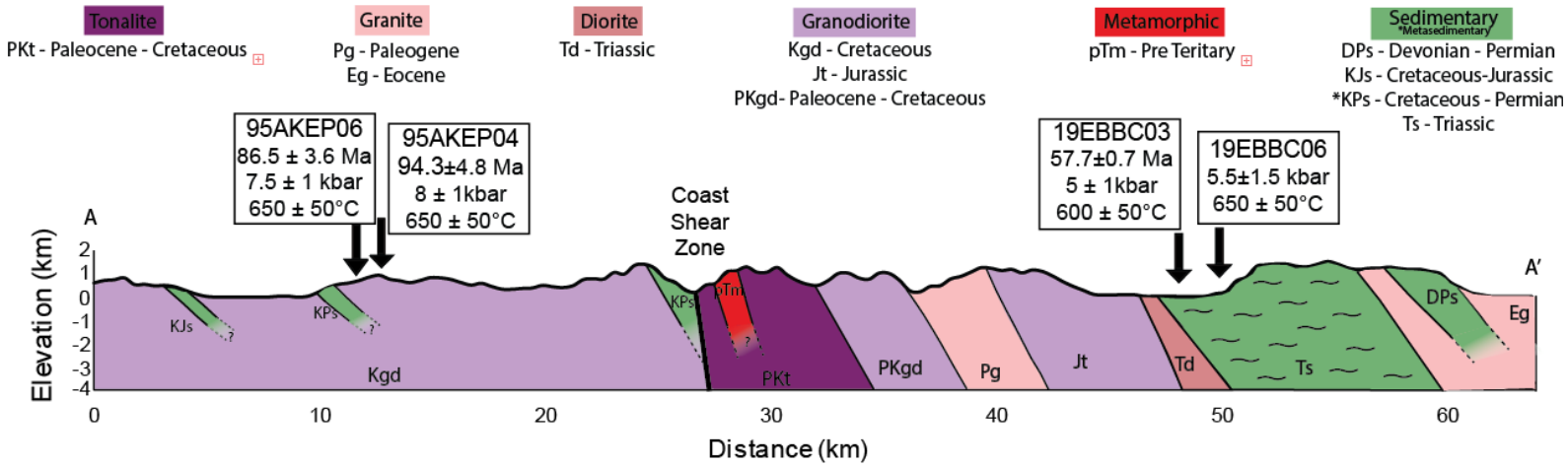

Figure 22. Schematic cross-section of the Stikine transect. In this interpretation, quartz diorite to granodiorite plutons are assumed to underlay a large part of the WMB; however, the extent of these bodies is likely overestimated. Samples and some structural data have been extrapolated from nearby locations from McClelland et al. (1991), Porter (1992), and Rusmore (personal comm).

CONCLUSION

This study presents new Sm-Nd ages for garnet growth and MADs to construct P-T-t paths for samples collected across the CMB in the Stikine River area. These data indicate that WMB metamorphism occurred at pressures that were at least 3 kbar greater than those in the EMB. Garnet growth was followed by > 24 km of exhumation in the WMB and > 14 km of exhumation in the EMB. Garnet growth ages and cooling rates further indicate that exhumation of the WMB occurred earlier than in the EMB; however, the exact timing is unknown. The CSZ is interpreted to have initiated as a reverse displacement fault associated with pre- to syn-90 Ma development of a west-directed orogenic wedge.

The data presented in this study fit into in broader, regional Coast Mountains picture. Implications regarding the sources, timing, and tempo of magma genesis in the mid-crustal roots of magmatic arcs can begin to be deduced from piecing together data points spread across the region. This study and data presented within indicate a deep crustal/mantle source of plutonism, similar to that observed in Mt. Waddington more than 725 km south. Metamorphism and plutonism near Mt. Waddington are attributed to a single regional-scale event spanning from 64-99 Ma, with several periods of unrelated amphibolite grade metamorphism and high-flux events, similar to characteristics of Stikine area metamorphism and plutonism. Magmatic sources just to the north of the Stikine transect, within the Stikine terrane, have old, crustal components. Further north, CGC pressures have been documented up to 10 kbar.

To further test the tectonic models proposed here, additional samples should be collected along the Stikine transect, specifically within the central CMB, to be analyzed for garnet Sm-Nd ages of metamorphism, zircon U-Pb ages of plutonism, and Bt and Hbl $^{40}Ar/^{39}Ar$, K-Ar cooling ages. Such additional data will help further constrain the spatial extent of various metamorphic and plutonic events across the CMB.

REFERENCES

Ague, J.J., 1991, Evidence for major mass transfer and volume strain during regional metamorphism of pelites: *Geology*, v. 19, p. 855-858.

Aleksey, M. E, Rusmore, M. E., Stowell, H. H., Cecil, M. R., Gutapfel, S. W., 2020, Evidence for the Northern Continuation of Eocene Crustal Extension, Northern Coast Mountains Batholith, British Columbia: *Geologic Society of America*, Abstract with Program, v. 5, No. 6.

Barton, M. et al., 1988, 'Mesozoic Contact Metamorphism in the Western United States', Ernst, W.G., eds., *Metamorphism and Crustal Evolution of the Western United States,* VII edn, Prentice Hall, Englewood, NJ, p. 110-178.

Baxter, E. F., Scherer, E. E., 2013, Garnet Geochronology: Timekeeper of Tectonometamorphic Processes: *Elements*, v. 9, p. 433–38.

Berg, H. C., Jones, D. L., Richter, D. H., 1972, Gravina-Nutzotin Belt; tectonic significance of an upper Mesozoic sedimentary and volcanic sequence in southern and southeastern Alaska: *US Geologic Survey. Professional Paper.*, v. 800, p. D1-D24.

Bollen, E. M., Stowell, H. H., Rusmore, M. E., Woodsworth, G. J., Cecil, M. R., 2022, The tempo of metamorphism and magmatism, Coast Mountains batholith, Canada: *Journal of Metamorphic Geology.*

Brew D.A. Ford A.B., 1981, The Coast Plutonic Complex sill, southeastern Alaska, in Albert N.R.D. Hudson T.L.eds.The U.S. Geological Survey in Alaska: Accomplishments during 1980 : U.S. Geological Survey Circular 823-B, p. B96–B98

Brew, D. A., Ford, A. B., 1978, Megalineament in southeastern Alaska marks southwest edge of Coast Range batholithic complex: *Canadian Journal of Earth Sciences*, v. 15, p. 1763-1772.

Carlson, W.D., 2006, Rates of Fe, Mg, Mn, and Ca diffusion in garnet: *American Mineralogist*, v. 91 p.1-11.

Carlson, W.D., 2012, Rates and mechanism of Y, REE, and Cr diffusion in garnet: *American Mineralogist*, v. *97*, p.1598-1618.

Cecil, M.R., Gehrels, G.E., Ducea, M.N., Patchett, P.J., 2011, U-Pb-Hf characterization of the central Coast Mountains batholith: Implications for petrogenesis and crustal architecture: *Lithosphere*, v.3, p.247-260.

Cook, R.D. and Crawford, M.L., 1994, Exhumation and tilting of the western metamorphic belt of the Coast orogen in southern southeastern Alaska: *Tectonics*, v. *13*, p.528-537.Chardon, D., Andronicos, C. L., Hollister, L.S., 1999, Large-scale transpressive shear zone patterns and displacements within magmatic arcs: The Coast Plutonic Complex, British Columbia: *Tectonics*, v. 18, p.278-292.

Crawford, M. L., Hollister, L. S., Woodsworth, G. J., 1987, Crustal deformation and regional metamorphism across a terrane boundary, Coast Plutonic Complex, British Columbia: *Tectonics*, v. 6, p. 343– 361.

Cui, Y., Miller, D., Schiarizza, P., and Diakow, L.J., 2017, British Columbia digital geology: *British Columbia Ministry of Energy, Mines and Petroleum Resources, British Columbia Geological Survey.* Open File, 2017-2018

de Capitani, C., Brown, T.H., 1987, The computation of chemical equilibrium in complex systems containing nonideal solutions: *Geochimica et Cosmochimica Acta*, v. 51, p. 2639–2652.

de Capitani, C., Petrakakis, K., 2010, The computation of equilibrium assemblage diagrams with Theriak/Domino software: *American Mineralogist*, v. 95, p. 1006–1016.

Evenchick, C.A., McMechan, M.E., McNicoll, V.J., and Carr, S.D., 2007, A synthesis of the Jurassic–Cretaceous tectonic evolution of the central and southeastern Canadian Cordillera: Exploring links across the orogen, Sears, J.W., Harms, T.A., and Evenchick, C.A., eds., *Whence the Mountains? Inquiries into the Evolution of Orogenic Systems: A Volume in Honor of Raymond A. Price*: Geological Society of America Special Paper 433, p. 117–145.

Ferry, J.M., Spear, F.S., 1978, Experimental calibration of the partitioning of Fe and Mg between biotite and garnet: *Contributions to Minerology and Petrology* v. 66, p. 113-117.

Gatewood, M.P., Dragovic, B., Stowell, H.H., Baxter, E.F., Hirsch, D.M., Bloom, R., 2015, Evaluating chemical equilibrium in metamorphic rocks using major element and Sm–Nd isotopic age zoning in garnet, Townshend Dam, Vermont, USA: *Chemical Geology*, v. 401, p.151-168.

Gehrels, G.E., and Berg, H.C., 1984, Geologic map of southeastern Alaska: *U.S. Geological Survey* Open-File Report 84-886.

Gehrels, G. E., McClelland, M. C., Samson, S. D., Patchett, P. J., Jackson, J. L., 1990, Ancient continental margin assemblage in the northern Coast Mountains, southeast Alaska and northwest Canada: *Geology*, v. 18, p. 208–211.

Gehrels, G.E., Saleeby, J. B., 1987, Geologic framework, tectonic evolution and displacement history of the Alexander Terrane: Tectonics, v. 6, p. 151-173.

Gehrels, G., Rusmore, M., Woodsworth, G., Crawford, M., Andronicos, C., Hollister, L., Patchett, J., Ducea, M., Butler, R., Klepeis, K., Davidson, C., 2009, U-Th-Pb geochronology of the Coast Mountains batholith in north-coastal British Columbia: Constraints on age and tectonic evolution: *Geological Society of America Bulletin*, v.121, p.1341-1361.

Ghent, E. D., Robbins, D. B., Stout, M. Z., 1979, Geothermometry, geobarometry and fluid compositions of metamorphosed calcsilicates and pelites, Mica Creek, British Columbia: *American Mineralogist*, v. 64, p. 874-885.

Greenwood, H.J., Woodsworth, G.J., Read, P.B., Ghent, E.D., and Evenchick, C.A., 1991, Metamorphism, Chapter 16, *in* Gabrielse, H.J. and Yorath, C.J. eds., Geology of the Cordilleran Orogen in Canada, *Geological Survey of Canada*, Geology of Canada, no. 4, p. 533–570.

Holland, T.J.B. and Powell, R., 1989. An internally consistent thermodynamic data set for phases of petrological interest: *Journal of Metamorphic Geology*, v. 16, p. 309–343.

Holland, T.J.B. & Powell, R., 2011, An improved and extended internally-consistent thermodynamic dataset for phases of petrological interest, involving a new equation of state for solids: *Journal of Metamorphic Geology*, v. 29, p. 333–383.

Hollister, L.S., 1966, Garnet zoning: an interpretation based on the Rayleigh fractionation model: *Science*, v.*154*, p.1647-1651.

Hollister, L.S., 1982, Metamorphic evidence for rapid (2 mm/yr) uplift of a portion of the Central Gneiss Complex, Coast Mountains, BC: *The Canadian Mineralogist* v.20, p.319-332.

Hollister, L.S., Andronicos, C., 'The Central Gneiss Complex, Coast Mountains, British Columbia' in Stowell, H.H., and McClelland, W.C., eds., *Tectonics of the Coast Mountains, Southeastern Alaska and British Columbia:* Boulder, Colorado, Geological Society of America Special Paper 343, p.45-60.

Hollister, L.S., Andronicos, C., 2000, The Central Gneiss Complex, Coast Mountains, British Columbia: Stowell, H.H. and McClelland, W.C., eds., *Tectonics of the Coast mountains, Southeastern Alaska and British Columbia*: Boulder, Colorado, Geological Society of America Special Paper 343.

Ingram, G.M. and Hutton, D.H., 1994, The Great Tonalite Sill: Emplacement into a contractional shear zone and implications for Late Cretaceous to early Eocene tectonics in southeastern Alaska and British Columbia: *Geological Society of America Bulletin*, v. *106*, p.715-728.

Klepeis, K.A., and Crawford, M.L., 1999, High-temperature arc-parallel normal faulting and transtension at the roots of an obliquely convergent orogen: *Geology*, v. 27, p. 7–10.

Kretz, R., 1983, Symbols for rock-forming minerals: *American Mineralogist*, v. 68, p. 77-279.

McClelland, W.C., 1992, Permian and older rocks of the southwestern Iskut River map area, northwestern British Columbia: *Geological Society of Canada*, Current Research Part A, Paper 92-1A, p. 303-307.

McClelland, W. C., Anovitz, L. M., Gehrels, G. E., 1990, Thermobarametric Constraints on the Structural Evolution of the Coast Mountains Batholith, Central Southeastern Alaska: *Canadian Journal of Earth Sciences*, v. 28, p. 912–28.

McClelland, W. C., Gehrels, G. E., Samson, S. D., Patchett, P. J., 1992, Structural and geochronologic relations along the western Flank of the Coast Mountains batholith: Stikine River to Cape Fanshaw, central southeastern Alaska: *Journal of Structural Geology*, v. 14, p. 475-489.

McClelland, W. C., Mattison, J. M., 1991, U-Pb (zircon) constraints on the age of the Yukon Tanana terrane in the Coast Mountains, central southeast Alaska and British Columbia: *Geological Society of America, Abstracts with Programs*, v. 23, p. A434.

Monger, J. W. H., Price, R. A., Templeman-Kluit, D. J., 1982, Tectonic accretion of the two major metamorphic and plutonic welts of the Canadian Cordillera: *Geology*, v. 10, p. 70-75.

Monger, J.W.H., Van der Heyden, P., Journeay, J.M., Evenchick, C.A., Mahoney, J.B., 1994, Jurassic-Cretaceous basins along the Canadian Coast Belt: Their bearing on pre-mid-Cretaceous sinistral displacements: *Geology*, 22, p.175-178.

Morozov, I.B., Smithson, S.B., Chen, J. and Hollister, L.S., 2001, Generation of new continental crust and terrane accretion in southeastern Alaska and western British Columbia: Constraints from P-and S-wave wide-angle seismic data (ACCRETE): *Tectonophysics*, v. 341, p.49-67.

Pearson, D. M., MacLeod, R. A., Ducea, M. N., Gehrels, G. E., Patchett, P. J., 2017, Sediment Underthrusting within a Continental Magmatic Arc: Coast Mountains Batholith, British Columbia: *Tectonics*, v. 36, p. 2022-2043.

Porter, S., 1992, Elbow Mountain crystalline complex, Iskut River map area, northwestern British Columbia: *Geological Survey of Canada*, Current Research, Part A, Paper 92-lA, p. 309-313.

Rubin, C. M., Saleeby, J. B., Cowan, D. S., Brandon, M. T., McGroder M. F., 1990, Regionally extensive mid-Cretaceous west-vergent thrust system in the northwestern Cordillera: Implications for continent-margin tectonism: *Geology*, v. 18, p. 276–280.

Rusmore, M. E., Woodsworth, G. J., 1994, Evolution of the eastern Waddington thrust belt and its relation to the mid-Cretaceous Coast Mountains arc, western British Columbia: *Tectonics*, v. 13, p. 1052-1067.

Rusmore, M. E., Woodsworth, G. J., and Gehrels, G. E., 2005, Two-stage exhumation of midcrustal arc rocks, Coast Mountains, British Columbia: *Tectonics*, v. 24, p. TC5013.

Shaw, D.M., 1956, Geochemistry of pelitic rocks. Part III: Major elements and general geochemistry: *Geological Society of America Bulletin,* v. 67, p. 919-934.

Sisson, V.B., 1985, Contact metamorphism and fluid evolution associated with the intrusion of the Ponder pluton, Coast Plutonic Complex, British Columbia, Canada, Ph.D. thesis: *Princeton, New Jersey, Princeton University*, p. 1-345.

Spear, F.S., 1993, 'The metamorphism of pelites' *Metamorphic Phase Equilibria and Pressure-Temperature-Time Paths,* 1, Mineralogical Society of America, Washington D.C., p. 337-391.

Stowell, H. H., 1989, Silicate and sulphide thermobarometry of low- to medium-grade metamorphic rocks from Holkham Bay, south-east Alaska: *Journal of Metamorphic Geology*, v. 7, p. 343-358.

Stowell, H.H., and Crawford, M. L., 2000, 'Metamorphic history of the Coast Mountains Oregon, western British Columbia and southeastern Alaska', in Stowell, H. H., and McClelland, W. C., eds., *Tectonics of the Coast mountains, Southeastern Alaska and British Columbia*: Boulder, Colorado, Geological Society of America Special Paper 343, p. 257-278.

Stowell, H. H., Goldberg, S. A., 1997, Sm-Nd garnet dating of polyphase metamorphism: Northern Coast Mountains, south-eastern Alaska, USA: *Journal of Metamorphic Geology*, v. 15, p. 439-450.

Stowell, H.H. and Hooper, R.J., 1990. Structural development of the western metamorphic belt adjacent to the Coast Plutonic Complex, southeastern Alaska: Evidence from Holkham Bay: *Tectonics*, v. 9, p.391-407.

Stowell, H.H., and Pike, M.A., 2000. A thermal model for cooling of foliated tonalite sill plutons, northern Coast Mountains, southeastern Alaska, *in* Stowell, H.H., and McClelland, W.C., eds. Tectonics of the Coast Mountains, Southeastern Alaska and British Columbia, *Geological Society of America Special Paper* 343, p. 183-192.

Stowell, H.H., Taylor, D.L., Tinkham, D.L., Goldberg, S.A. and Ouderkirk, K.A., 2001, Contact metamorphic *P–T–t* paths from Sm–Nd garnet ages, phase equilibria modelling and thermobarometry: Garnet Ledge, south-eastern Alaska, USA: *Journal of Metamorphic Geology*, v. 19, p. 645-660.

Stowell, H. H.,Tinkham, D. K., 2003, Integration of Phase Equilibria Modelling and Garnet Sm-Nd Chronology for Construction of P-T-t Paths: Examples from the Cordilleran Coast Plutonic Complex, USA: *Geological Society Special Publication*, v. 220, p. 119–145.

Tinkham, D. K., 2021, *Phase Equilibria with THERIAK-DOMINO,* viewed 3 May 2022, <https://dtinkham.net/peq.html>

van der Heyden, P. 1992, A Middle Jurassic to early Tertiary Andean-Sierran arc model for the Coast belt of British Columbia*: Tectonics,* v. 11, p. 82–97.

Vermeesch, P., 2018, IsoplotR: a free and open toolbox for geochronology: *Geoscience Frontiers*, v. 9, p. 1479-1493.

Wood, D.J., Stowell, H.H., Onstott, T.C., and Hollister, L.S., 1991. $^{40}Ar/^{39}Ar$ Constraints on the emplacement, uplift, and cooling of the Coast Plutonic Complex sill, SE Alaska. *Geological Society of America Bulletin,* 103, 849-860.

Woodsworth, G. J., Rusmore, M. E., Stowell, H. H., Hollister, L. S., 2020, 'Architecture and Evolution of the Crust during Continental Arc Magmatism: A transect through the Coast Mountains Batholith, British Columbia: *Geological Society of American Field Guide,* v. 58, p. 1-4.

APPENDIX 1: COMPLETE LIST OF PREDICTED MINERAL ASSEMBLAGES ON P-T MADS

Figure 8. 95AKEP04

Stable fields:

1. Grt, Chl, WM (2), Mrg, Qtz, H2O, Spn
2. Grt, Bt, Sil, Liq, Qtz, Rt
3. Grt, Bt, Pl, Ky, Liq, H2O, Qtz, Rt
4. Grt, Chl, (2) WM, Rt, H2O, Qtz, Mrg, Spn
5. Grt, Bt, (2) WM, St, Sil, Qtz, H2O
6. Grt, Bt, Pl, Ky, St, Rt, Qtz, H2O
7. Grt, Bt, Pl, Ky, Rt, Qtz, H2O
8. Grt, Bt, Pl, Sil, Rt, Liq, H2O
9. Grt, Bt, Pl, Ilm, St, Sil, Qtz, H2O
10. Grt, Bt, Pl, Ilm, Sil, Qtz, H2O
11. Grt, Bt, Pl, Sil, Ilm, Qtz, Liq, H2O
12. Grt, Bt, Pl, Ilm, Crd, Sil, Qtz, Liq, H2O
13. Grt, Bt, Pl, Ilm, Crd, Qtz, Liq
14. Grt, Bt, PlSil, Ilm, Crd, Qtz, Liq
15. Grt, Ilm, Crd, Qtz, Liq
16. Grt, Crd, Sil, Rt, Qtz, Liq
17. Grt, Chl, Pl, WM, Ilm, Qtz, H2O
18. Grt, Bt, Pl, Ilm, Crd, Sil, Qtz, H2O

Figure 12. 95AKEP06

Stable fields:

1. Grt, bt, chl, WM (2), cpx, ab, sph, qtz
2. Grt, bt, chl, WM (2), cpx, sph, qtz, H2O
3. Grt, bt, chl, WM (2), sph, qtz, H2O
4. Grt, bt, chl, WM (2), camp, sph, qtz, H2O
5. Grt, bt, chl, WM (2), rt, camp, sph, qtz, H2O
6. Grt, bt, chl, WM, rt, camp, qtz, H2O
7. Grt, bt, st, rt, WM, pl, qtz, H2O
8. Grt, bt, st, rt, pl, qtz, H2O
9. Grt, bt, ky, rt, pl, qtz, H2O

10. Grt, bt, ky, rt, pl, qtz, H2O, liq
11. Grt, bt, ky, rt, pl, qtz, liq
12. Grt, bt, sil, rt, pl, qtz, liq
13. Grt, bt, chl, WM, rt, pl, qtz, H2O
14. Grt, bt, chl, WM(2), rt, pl, qtz, H2O
15. Grt, bt, ky, rt, pl, qtz, liq, H2O
16. Grt, bt, chl, WM, rt, pl, qtz, H2O
17. Grt, bt, chl, WM, st, rt, pl, qtz, H2O
18. Grt, bt, sil, rt, pl, qtz, liq, H2O
19. Grt, bt, sill, rt, crd, pl, qtz, liq
20. Grt, bt, Rt, crd, pl, qtz, liq
21. Grt, crd, qtz, rt, liq
22. Grt, rt, crd, liq
23. Grt, chl, WM, ab, sph, qtz, H2O
24. Grt, chl, WM(2), ab, sph, qtz, H2O
25. Grt, bt, chl, WM (2), sph, pl, qtz, H2O
26. Bt, chl, rt, ilm, WM (2), pl, qtz, H2O
27. Grt, bt, chl, pl, qtz, ilm, WM (2), H2O
28. Grt, bt, chl, WM, ilm, st, pl, qtz, H2O
29. Grt, bt, chl, ilm, st, pl, qtz, H2O
30. Grt, bt, ilm, st, pl, qtz, H2O
31. Grt, bt, ilm, sil, pl, qtz, H2O
32. Grt, bt, ilm, sil, pl, qtz, H2O, liq
33. Grt, bt, sill, ilm, crd, pl, qtz, liq
34. Grt, bt, ilm, crd, pl, qtz, liq
35. Grt, bt, ilm, crd, pl, liq
36. Bt, chl, WM, ab, sph, pl, qtz, H2O
37. Bt, chl, rt, WM, pl, qtz, H2O
38. Bt, chl, rt, ilm, WM, pl, qtz, H2O
39. Bt, chl, ilm, WM, pl, qtz, H2O
40. Bt, chl, ilm, WM (2), pl, qtz, H2O
41. Grt, bt, ilm, crd, sil, pl, qtz, H2O
42. Grt, bt, ilm, crd, sill, pl, qtz, H2O, liq
43. Grt, bt, ilm, crd, pl, qtz, H2O, liq
44. Grt, ilm, crd, pl, liq
45. Grt, bt, ilm, crd, pl, qtz, H2O

Figure 16. 19EBBC03

Stable fields:

1. Grt, bt, chl, WM, ab, sph, czo, qtz, H2O
2. Grt, bt, chl, WM (2), sph, czo, qtz, H2O
3. Grt, bt, chl, WM(2), czo, rt, qtz, H2O
4. Grt, bt, chl, WM (2), ilm, czo, rt, qtz, H2O
5. Grt, bt, WM, mrg, czo, rt, pl, qtz, H2O
6. Grt, bt, ky, rt, pl, qtz, H2O
7. Grt, bt, rt, pl, qtz, H2O, liq
8. Grt, Bt, rt, pl, qtz, liq
9. Grt, rt, pl, qtz, liq
10. Grt, bt, chl, WM (2), czo, ilm, qtz, H2O
11. Grt, bt, chl, rt, czo, mrg, pl, qtz, H2O
12. Grt, Bt, rt, czo, mrg, pl, qtz, H2O
13. Grt, bt, rt, mrg, pl, qtz, H2O
14. Grt, bt, rt, sill, pl, qtz, H2O
15. Grt, bt, rt, pl, qtz, H2O
16. Grt, bt, rt, ilm, pl, qtz, H2O, liq
17. Grt, bt, rt, ilm, pl, qtz, liq
18. Grt, bt, chl, WM, czo, ilm, pl, qtz, H2O
19. Grt, bt, chl, czo, ilm, mrg, pl, qtz, H2O
20. Grt, bt, chl, ilm, mrg, pl, qtz, H2O
21. Grt, bt, st, ilm, pl, qtz, H2O
22. Grt, bt, ilm, sill, pl, qtz, H2O
23. Grt, bt, ilm, pl, qtz, H2O
24. Grt, bt, ilm, pl, qtz, H2O, liq
25. Grt, bt, ilm, pl, qtz, liq
26. Grt, ilm, pl, qtz, liq
27. Grt, ilm, pl, liq
28. Grt, bt, chl, czo, WM, sph, pl, qtz, H2O
29. Grt, bt, chl, ilm, st, pl, qtz, H2O
30. Grt, bt, ilm, crd, pl, qtz, H2O
31. Grt, bt, ilm, crd, pl, qtz, H2O, liq
32. Grt, bt, ilm, crd, pl, liq
33. Grt, ilm, crd, pl, liq

Figure 20. 19EBBC06F

Stable fields:

1. Chl, WM (2), ab, czo, sph, qtz, H2O
2. Bt, chl, WM (2), czo, rt, sph, qtz, H2O
3. Bt, chl, WM (2), czo, rt, qtz, H2O
4. Grt, bt, chl, WM (2), czo, rt, qtz, H2O
5. Grt, bt, WM (2), rt, mrg, pl, qtz, H2O
6. Grt, bt, WM (2), st, rt, pl, qtz, H2O
7. Grt, bt, ky, rt, pl, qtz, H2O
8. Grt, bt, ky, rt, pl, qtz, H2O, liq
9. Grt, bt, ky, rt, pl, qtz, liq
10. Grt, bt, sill, rt, pl, qtz, liq
11. Grt, sill, rt, pl, qtz, liq
12. Bt, chl, WM, rt, pl, qtz, H2O
13. Bt, chl, WM, rt, ilm, pl, qtz, H2O
14. Bt, chl, WM, ilm, pl, qtz, H2O
15. Bt, chl, WM (2), ilm (2), pl, qtz, H2O
16. Grt, bt, chl, WM (2), ilm (2), pl, qtz, H2O
17. Bt, WM (2), st, rt, pl, qtz, H2O
18. Grt, bt, st, ky, rt, pl, qtz, H2O
19. Grt, bt, st, ky, ilm, pl, qtz, H2O
20. Grt, bt, ky, ilm, pl, qtz, H2O
21. Grt, bt, sill, ilm, pl, qtz, H2O
22. Grt, bt, sill, ilm, pl, qtz, H2O, liq
23. Grt, bt, sill, ilm, pl, qtz, liq
24. Grt, bt, sill, rt, crd, pl, qtz, liq
25. Grt, sill, rt, crd, pl, qtz, liq
26. Bt, sill, st, ilm, pl, qtz, H2O
27. Bt, sill, st, ilm (2), pl, qtz, H2O
28. Grt, bt, sill, ilm, crd, pl, qtz, H2O
29. Grt, bt, sill, crd, ilm, pl, qtz, H2O, liq
30. Grt, bt, sill, crd, ilm, pl, qtz, liq
31. Grt, bt, ilm, crd, pl, qtz, liq
32. Grt, ilm, crd, pl, qtz, liq
33. Bt, and, ilm, crd, pl, qtz, H2O
34. Bt, sill, ilm, crd, pl, qtz, H2O
35. Bt, sill, ilm, crd, pl, qtz, H2O, liq
36. Bt, ilm, crd, pl, qtz, liq
37. Ilm, crd, pl, qtz, liq